

Entanglement patterns and generalized correlation functions in quantum many-body systems

G. Barcza¹, R. M. Noack², J. Sólyom¹, Ö. Legeza¹

¹ *Strongly Correlated Systems “Lendület” Research group,*

Wigner Research Centre for Physics, H-1525 Budapest, Hungary

² *Fachbereich Physik, Philipps-Universität Marburg, 35032 Marburg, Germany*

(Dated: July 30, 2021)

We introduce transition operators that in a given basis of the single-site states of a many-body system have a single non-vanishing matrix element and introduce their correlation functions. We show that they fall into groups that decay with the same rate. The mutual information defined in terms of the von Neumann entropy between two sites is given in terms of these so-called generalized correlation functions. We confirm numerically that the long-distance decay of the mutual information follows the square of that of the most slowly decaying generalized correlation function. The main advantage of our procedure is that, in order to identify the most relevant physical processes, there is no need to know *a priori* the nature of the ordering in the system, i.e., no need to explicitly construct particular physical correlation functions. We explore the behavior of the mutual information and the generalized correlation functions for conformally invariant models and for the $SU(n)$ Hubbard model with $n = 2, 3, 4$, and 5 , which are, in general, not conformally invariant. In this latter case, we show that for filling $f = 1/q$ and $q < n$, the ground state consists of highly entangled q -site units that are further entangled by single bonds. In addition, we extend the picture of the two-site mutual information and the corresponding generalized correlation functions to the n -site case.

I. INTRODUCTION

Phases of many-body systems are often characterized in terms of the long-distance behavior of spatial correlation functions.^{1,2} In particular, the decay of a correlation function to a finite value at long distance is characteristic of an ordered phase, exponential decay indicates a gapped or disordered phase, while power-law decay is a characteristic feature of critical systems. In quantum systems, entanglement-based measures can also be used to characterize phases.^{3,4} In the past decade, much effort has been devoted to developing and understanding quantitative measures of entanglement.^{5–8} Our goal here is to elucidate the relationship between traditional correlation functions and such entanglement-based measures of quantum correlations.

The full description of a quantum mechanical system can be given in a pure state by the wavefunction, $|\Psi\rangle$, or in a mixed state by the density matrix, ρ . For a bipartite system in a pure state, information on the entanglement of the two parts of the system is encoded in the reduced density matrix of one subsystem, $\rho_A = \text{Tr}_B |\Psi\rangle\langle\Psi|$, where we label the subsystem of interest by A and the other subsystem by B , and Tr_B means carrying out the trace over subsystem B . The eigenvalue spectrum of ρ_A completely characterizes the entanglement between subsystems A and B . A number of quantitative measures of entanglement can be extracted from the eigenvalue spectrum.^{7,8} The most commonly used measure is the von Neumann entropy^{9,10}

$$s_A = -\text{Tr} \rho_A \ln \rho_A; \quad (1)$$

others include the more general Rényi entropy,¹¹ the

concurrence,⁶ and the Schmidt number. Once the eigenvalues w_α of ρ_A are known, the von Neumann entropy can be calculated using $s_A = -\sum_\alpha w_\alpha \ln w_\alpha$.

The Hilbert space of a finite many-body quantum system is formed by taking the tensor product of simple building-block systems, which will be called “sites”; here we generally take the sites to be local units with “finite Hilbert spaces” on a regular lattice. In Eq. (1), subsystem A can be formed, in general, from an arbitrary subset of the total set of sites. While the usual practice is to take one, two, or more neighboring sites, it can also be useful to form it from non-adjacent sites.¹²

The number of sites included and where they are located on the lattice can be tailored to obtain specific information on the distribution of entanglement on the lattice, which can then be used to characterize the physical nature of the quantum phase of the system. For example, the scaling behavior of the von Neumann entropy of a contiguous block of sites with the number of sites has been used to study the quantum phases of one-dimensional systems. For systems with local interactions, this “block entropy” diverges logarithmically with block size for critical systems, but saturates for gapped systems,^{13,14} and it has more complex behavior when non-local interactions are present.^{15,16}

The entropy of particular subsystems such as the single-site, the nearest-neighbor two-site, and the block entropy as a function of microscopic control parameters can be used to detect and characterize many classes of quantum phase transitions.^{5,14,17–22} However, since topological states cannot be described by local order parameters, quantum phase transitions to such states must be detected by alternative means.^{23–28} For example, for two-dimensional systems with topological order such as the

Heisenberg model on a kagome lattice, deviations of the block entropy from area-law scaling can be used to detect topologically ordered phases.^{29–31} In addition, a gap in the entanglement spectrum can be used to characterize topological order.³²

In the cases discussed above, the entanglement has been measured between two subsystems of a bipartite partition of the total system. Thus, it characterizes all correlations of quantum origin when the total system is in a pure state. While the dependence of these subsystem entropies on size and placement on the lattice can yield some information on spatial properties, they do not contain specific information on the entanglement between sites.

Taking into account the amount and structure of entanglement between different part of a large system is also very important in developing numerical algorithms based on tensor product approximations.^{33–47} Since the computational cost of all of these methods is determined by the rank of the matrices^{15,48} and tensors,⁴⁹ it is crucial to obtain as much knowledge as possible about the entanglement structure of the system under study and to incorporate this knowledge in the matrix or tensor structure of the state used to simulate it.⁴⁷

In the present paper, we will consider correlations between two sites. Since these sites are embedded in a larger system, they are, in general, in a mixed state, leading to a more complicated picture of the origin of the correlations. The correlations can be of classical or of quantum origin; moreover, there are quantum correlations which are not due to entanglement.⁵⁰ A useful quantity to numerically characterize all kinds of correlations between pairs of sites is the mutual information

$$I_{ij} = s_i + s_j - s_{ij}, \quad (2)$$

calculated between two generally placed sites, i and j . Here s_i is the von Neumann entropy defined in Eq. (1), where now a subsystem A is chosen to be the single site i , and s_{ij} is the entropy of the subsystem consisting of sites i and j . The mutual information I_{ij} describes the correlation between sites i and j embedded in a larger system. When studied for all pairs i and j , it yields a weighted graph of the overall correlations of both classical and quantum origin in the lattice. The mutual information defined in this way has been used previously to study correlation between neighboring sites in spin and fermionic chains with local interactions⁵¹ and in quantum chemical problems.^{16,52–56} Here we will study its relationship to conventional two-point correlation functions in quantum lattice models.

We will introduce transition operators that in a given basis of single-site states of a many-body system have a single non-vanishing matrix element. We will then show that the matrix elements of the two-site density matrix needed to calculate the mutual information can be expressed in terms of expectation values of transition operators. These matrix elements have the form of *general-*

ized correlation functions and contain, by definition, all two-site correlations. Thus, there is no need for *a priori* knowledge about the nature of the ordering in the system, i.e., no need to explicitly construct particular physical correlation functions. The two-site mutual information in terms of the von Neumann entropy consists of a weighted average of generalized correlation functions and, in fact, measures the strength of the overall correlation between sites i and j . In the following, we will call this an “entanglement bond” if it is larger than a pre-defined threshold value, chosen here to be 10^{-1} . The two-site mutual information, however, does not explicitly tell us what physical process is responsible for the entanglement in the system. The task, then, is to relate the generalized correlation functions to physically motivated correlation functions such as spin-spin, density-density, electron-hole, or pairing correlation functions.

Within the context of a discussion of the entropy area law for classes of classical and quantum lattice models with short-range Hamiltonians, Wolf *et al.*⁵⁷ derived an inequality (their Eq. (5)) in which the mutual information of two spatially separated regions is bounded from below by the (appropriately normalized) square of any connected correlation function between local operators in the two regions. The implication is that the equality holds at large separations when the most slowly decaying correlation function is inserted. Our study of the two-site mutual information finds that the equality does indeed apply for the most slowly decaying correlation function, consistent with this bound. In addition, for conformally invariant systems, Furukawa *et al.*⁵⁸ studied the behavior of the mutual information of two separated subsystems of general size and related its behavior to the square of the exponent of the leading algebraic decay of the two-point correlation functions. Our findings below for conformally invariant phases are consistent with this result.

In summary, our goal is, on the one hand, to provide an explicit scheme for efficiently constructing the two-site mutual information for the the density-matrix renormalization group (DMRG) and other matrix-product-state-(MPS)-based methods and, on the other, to investigate its behavior for several conformally and non-conformally-invariant models to make contact with the theoretical predictions in Refs. 57 and 14.

The paper is organized as follows. In Sec. II, we describe the theoretical background. In Sec. III, we demonstrate our approach on the one-dimensional, spin-1/2, anisotropic Heisenberg model. In Sec. IV, we present the spatial entanglement pattern for the $SU(n)$ Hubbard model at various commensurate fillings and, based on the generalized correlation functions, identify the underlying relevant physical processes. Finally, Sec. V contains our conclusions.

II. THE ONE- AND TWO-SITE DENSITY MATRIX

A. One-site density matrix and the transition operators

The N -site wave function can be written in terms of the single-site q -dimensional basis as

$$|\Psi\rangle = \sum_{\alpha_1, \dots, \alpha_N} C_{\alpha_1, \dots, \alpha_N} |\alpha_1\rangle \dots |\alpha_N\rangle, \quad (3)$$

where the α_j denote single-site basis states and the set of coefficients $C_{\alpha_1, \dots, \alpha_N}$ can be viewed as an N th-order tensor. Matrix elements of the single-site density matrix $\langle \alpha'_i | \rho_i | \alpha_i \rangle$ are calculated by taking the trace of $|\Psi\rangle\langle\Psi|$ over all local bases except for α_i , the bases of sites i . The dimension of C grows exponentially with system size N ; thus, such full tensor representations of the wave function are only possible for small system sizes. Fortunately, the N th-order tensor C can, in many cases, be efficiently factorized into a product of matrices, $C_{\alpha_1, \dots, \alpha_N} = A_{\alpha_1} \dots A_{\alpha_N}$, leading to a MPS representation of the wave function, where the A_{α_i} are $M \times M$ matrices in general.³⁸ For systems with open boundary conditions, A_{α_1} and A_{α_N} are row and column vectors, respectively. In the MPS representation, the calculation of ρ_i is straightforward as it corresponds to the contraction of the network over all states except those at site i . A diagram depicting such a contraction for a finite, $N = 8$ -site system is shown in Fig. 1. In the MPS-based

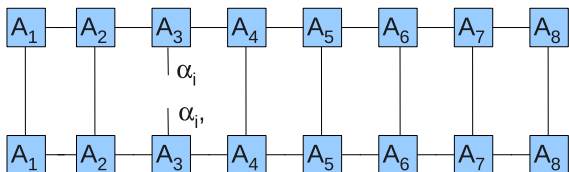


FIG. 1. Contraction of the MPS network to calculate the one-site reduced density matrix for a chain with $N = 8$.

two-site DMRG method, the system is divided into four subsystems, and $|\Psi\rangle$ is formed from the tensor products of the corresponding Hilbert spaces (see Ref. [34]). For a given partitioning, expectation values can be calculated within the multi-site block basis.

In general, the trace to obtain ρ_i , as carried out over the MPS wave function can be decomposed into a sum of projection operators related to the bases described by the free variables α_i . That is, the matrix representation of the one-site reduced density matrix $\langle \alpha'_i | \rho_i | \alpha_i \rangle$ can be constructed from operators describing transitions between the single-site basis $|\alpha_i\rangle$.

For a q -dimensional local Hilbert space, we can represent transitions between the basis states using q^2 possible transition operators $\mathcal{T}^{(m)}$ with $m = 1 \dots q^2$. The structure of the $q \times q$ operators $\mathcal{T}^{(m)}$ is simple: each operator contains only a single non-vanishing matrix el-

ement with the value one at position α' , α , where $|\alpha\rangle$ is the initial state and $|\alpha'\rangle$ is the final state; explicitly, $(\mathcal{T}^{(m)})_{\alpha', \alpha} = \delta_{\alpha + q[\alpha' - 1], m}$. It thus acts like a transition matrix between state $|\alpha\rangle$ and $|\alpha'\rangle$, $\mathcal{T}^{(m)}|\alpha\rangle = |\alpha'\rangle$, for $\alpha = (m-1) \bmod q + 1$ and $\alpha' = \lfloor (m-1)/q \rfloor + 1$, where $\lfloor x \rfloor$ denotes the floor function, the integral part of x . These operators can be extended to operate on the complete Hilbert space consisting of N local Hilbert spaces labeled by $i = 1, \dots, N$ as

$$\mathcal{T}_i^{(m)} = \bigotimes_{j=1}^{i-1} \mathbb{1} \otimes \mathcal{T}^{(m)} \otimes \bigotimes_{j=i+1}^N \mathbb{1}, \quad (4)$$

where the operators on the right-hand side act on the appropriate local single-site basis, and $\mathbb{1}$ is the identity operator on the local basis.

For the many-electron wave function, the matrix elements of the one-site reduced density matrices can be expressed in terms of expectation values of $\mathcal{T}_i^{(m)}$ operators acting on specific sites. When the individual local states are completely distinguished by abelian quantum numbers, the one-site density matrix is diagonal and has the form $\langle \alpha'_i | \rho_i | \alpha_i \rangle = \delta_{\alpha_i, \alpha'_i} \langle \mathcal{T}_i^{(\alpha_i(q+1)-q)} \rangle$, where the expectation values are calculated using the N -site many-body state. Once the one-site reduced density matrix ρ_i is constructed, s_i can be determined from its eigenvalues, which are the selected expectation values themselves, hence $s_i = -\sum_{l=1}^q \langle \mathcal{T}_i^{l(q+1)-q} \rangle \times \ln \langle \mathcal{T}_i^{l(q+1)-q} \rangle$.

B. Two-site density matrix and the generalized correlation functions

We now consider the two-site reduced density matrix ρ_{ij} . It can be calculated by taking the trace of $|\Psi\rangle\langle\Psi|$ over all local bases except for α_i and α_j , the bases of sites i and j . In the MPS representation, the calculation of ρ_{ij} corresponds to product of bra- and ket-MPS with two sites left uncontracted. Its matrix elements $\langle \alpha'_i, \beta'_j | \rho_{ij} | \alpha_i, \beta_j \rangle$ mediate a transition from state $|\alpha_i, \beta_j\rangle$ to state $|\alpha'_i, \beta'_j\rangle$, where α_i and α'_i label the initial and final states, respectively, on spatial site i and β_j and β'_j the initial and final states, respectively, on spatial site j . Thus, ρ_{ij} can be calculated from expectation values of operator products $\mathcal{T}_i^{(m)} \mathcal{T}_j^{(n)}$. Here the two q -dimensional spaces for states defined on sites i and j are expressed as one q^2 -dimensional space. Since the operators $\mathcal{T}_i^{(m)}$ can be expressed in terms of localized spin and fermion operators, the two-site reduced density matrix ρ_{ij} can be built explicitly from the expectation values of two-site operator products. The two-site reduced density matrix ρ_{ij} has non-zero matrix elements only between two-site states possessing the same quantum numbers because ρ_{ij} does not change the quantum numbers of the two sites (i.e., ρ_{ij} is block-diagonal in the two-site product basis), reducing the number of matrix elements that need be calculated. The symmetry properties of ρ_{ij} further reduce

the number of expectation values to be determined.

Once the two-site reduced density matrix ρ_{ij} is constructed, s_{ij} can be determined from its eigenvalues $w_{ij,\alpha}$, and the mutual information can be calculated using Eq. (2). An important feature of this method is that one can also analyze the sources of entanglement encoded in I_{ij} by studying the behavior of the matrix elements of ρ_{ij} . We term the expectation values of pairs of state-transition operators, $\langle \mathcal{T}_i^{(m)} \mathcal{T}_j^{(n)} \rangle = \langle \Psi | \mathcal{T}_i^{(m)} \mathcal{T}_j^{(n)} | \Psi \rangle$, *generalized correlation functions* in order to distinguish them from conventional correlation functions, i.e., those based on physically motivated operators such as local spin or density operators. This is a generalization of the procedure introduced in the DMRG context for spin-1/2 fermion models in Refs. 52 and 55. As we will see below, they can be used to identify the relevant physical processes that lead to the generation of the entanglement. This procedure will be demonstrated on the spin-

1/2 Heisenberg model and on the $SU(n)$ Hubbard model for $n \geq 2$.

It is important to take into account that when ρ_{ij} is calculated, the system is decomposed into three subsystems. For a tripartite system, the wave function can be written

$$|\Psi\rangle = \sum_{\alpha_i, \alpha_j, \beta} C_{\alpha_i, \alpha_j, \beta} |\alpha_i\rangle |\alpha_j\rangle |\beta\rangle, \quad (5)$$

where α_i and α_j label the bases of the sites i and j , and β labels the basis of the environment, which is composed of the remaining sites. A given generalized correlation function describes the transition from a particular initial state to a particular final state. It can be expressed in terms of the coefficients of the corresponding wave function in the tripartite basis as

$$\langle \mathcal{T}_i^{(m)} \mathcal{T}_j^{(n)} \rangle = \sum_{\alpha'_i, \alpha'_j, \beta'} \sum_{\alpha_i, \alpha_j, \beta} C_{\alpha'_i, \alpha'_j, \beta'}^* C_{\alpha_i, \alpha_j, \beta} \langle \alpha'_i | \langle \alpha'_j | \langle \beta' | \mathcal{T}_i^{(m)} \mathcal{T}_j^{(n)} | \alpha_i \rangle | \alpha_j \rangle | \beta \rangle = \sum_{\beta} C_{l(m), l(n), \beta}^* C_{r(m), r(n), \beta}, \quad (6)$$

where $r(m) = (m-1) \pmod{q} + 1$ and $l(m) = \lfloor (m-1)/q \rfloor + 1$. A given generalized correlation function measures the amplitude in the wavefunction within a particular environment. For example, it can be used to characterize the singlet valence bond between sites with spin-1/2 degrees of freedom.

In general, $\langle \mathcal{T}_i^{(m)} \mathcal{T}_j^{(n)} \rangle$ contains both connected and disconnected contributions between subsystems i and j . Therefore, it can, in general, scale to a finite value as the distance $l = |i-j|$ is increased. Note that this can occur even if the many-body state is not characterized by long-range order, i.e., even if the physical correlation function goes to zero for large l . In order to circumvent this behavior, we generally study the connected part of the generalized correlation functions,

$$\langle \mathcal{T}_i^{(m)} \mathcal{T}_j^{(n)} \rangle_C = \langle \mathcal{T}_i^{(m)} \mathcal{T}_j^{(n)} \rangle - \langle \mathcal{T}_i^{(m)} \rangle \langle \mathcal{T}_j^{(n)} \rangle, \quad (7)$$

where the disconnected part, given by the product of the expectation values of the local transition operators, is subtracted out. Note that in Eq. (2), the mutual information is formulated in such a way that the disconnected parts of the general correlation functions do not contribute. However, there is no way to express I_{ij} directly as a function of the connected parts of the generalized correlation functions.

The spatial behavior of the correlation functions depends essentially on the type of intermediate states for which the matrix elements of $\mathcal{T}_i^{(m)}$ and $\mathcal{T}_j^{(n)}$ are finite between these states and the ground state. Different $\mathcal{T}_i^{(m)}$ operators may transfer the ground state to the same in-

termediate state and, therefore, different generalized correlation functions may have similar properties. Therefore, we can classify the generalized correlation functions according to their type of decay. This behavior will also be investigated in detail in the following sections. Note that the decay properties of two-site correlation functions can also be obtained from the transfer operator used in the MPS framework.^{59,60}

C. Example: spin-1/2 case

As an example, we first consider a spin-1/2 model. The local Hilbert space is two-dimensional and is spanned by the spin-up basis state $|\uparrow\rangle$ and the spin-down basis state $|\downarrow\rangle$. The action of the four possible $\mathcal{T}^{(m)}$ (for $m = 1 \dots 4$) and their representations as standard one-site operators are given as

$$\begin{aligned} \mathcal{T}_i^{(1)} &= |\downarrow\rangle\langle\downarrow| = -S_i^z + \frac{1}{2}\mathbb{1}, & \mathcal{T}_i^{(2)} &= |\downarrow\rangle\langle\uparrow| = S_i^-, \\ \mathcal{T}_i^{(3)} &= |\uparrow\rangle\langle\downarrow| = S_i^+, & \mathcal{T}_i^{(4)} &= |\uparrow\rangle\langle\uparrow| = S_i^z + \frac{1}{2}\mathbb{1}. \end{aligned} \quad (8)$$

Using these definitions, we can express the physical correlation functions, G_{ij} , directly in terms of the gener-

alized correlation functions,

$$\begin{aligned}
G_{ij}^{xx} &= \langle S_i^x S_j^x \rangle = \frac{1}{4} \left(\langle \mathcal{T}_i^{(2)} \mathcal{T}_j^{(3)} \rangle + \langle \mathcal{T}_i^{(3)} \mathcal{T}_j^{(2)} \rangle \right. \\
&\quad \left. + \langle \mathcal{T}_i^{(2)} \mathcal{T}_j^{(2)} \rangle + \langle \mathcal{T}_i^{(3)} \mathcal{T}_j^{(3)} \rangle \right), \\
G_{ij}^{yy} &= \langle S_i^y S_j^y \rangle = \frac{1}{4} \left(\langle \mathcal{T}_i^{(2)} \mathcal{T}_j^{(3)} \rangle + \langle \mathcal{T}_i^{(3)} \mathcal{T}_j^{(2)} \rangle \right. \\
&\quad \left. - \langle \mathcal{T}_i^{(2)} \mathcal{T}_j^{(2)} \rangle - \langle \mathcal{T}_i^{(3)} \mathcal{T}_j^{(3)} \rangle \right), \\
G_{ij}^{zz} &= \langle S_i^z S_j^z \rangle = \frac{1}{4} \left(\langle \mathcal{T}_i^{(1)} \mathcal{T}_j^{(1)} \rangle + \langle \mathcal{T}_i^{(4)} \mathcal{T}_j^{(4)} \rangle \right. \\
&\quad \left. - \langle \mathcal{T}_i^{(1)} \mathcal{T}_j^{(4)} \rangle - \langle \mathcal{T}_i^{(4)} \mathcal{T}_j^{(1)} \rangle \right). \quad (9)
\end{aligned}$$

For the most general spin Hamiltonian, all generalized correlation functions might be different. In the following, we will consider the XXZ Heisenberg model (see Eq. (15)) $\langle \mathcal{T}_i^{(2)} \mathcal{T}_j^{(2)} \rangle = \langle \mathcal{T}_i^{(3)} \mathcal{T}_j^{(3)} \rangle = 0$ and $\langle \mathcal{T}_i^{(2)} \mathcal{T}_j^{(3)} \rangle = \langle \mathcal{T}_i^{(3)} \mathcal{T}_j^{(2)} \rangle$. In addition, due to up-down symmetry in the region $-1 < \Delta < 1$, $\langle \mathcal{T}_i^{(1)} \mathcal{T}_j^{(1)} \rangle$, $\langle \mathcal{T}_i^{(1)} \mathcal{T}_j^{(4)} \rangle$, $\langle \mathcal{T}_i^{(4)} \mathcal{T}_j^{(1)} \rangle$, $\langle \mathcal{T}_i^{(4)} \mathcal{T}_j^{(4)} \rangle$ are not independent and they are related to $\langle S_i^z \rangle$ and $\langle S_j^z \rangle$. On the other hand, as was mentioned earlier, the matrix elements of ρ_{ij} can be expressed in terms of the same generalized correlation functions. The non-vanishing matrix elements are shown for the XXZ model in Table I, where, for easier readability, the notation m/n is used for $\langle \mathcal{T}_i^{(m)} \mathcal{T}_j^{(n)} \rangle$.

ρ_{ij}	$ \downarrow\rangle_i \downarrow\rangle_j$	$ \downarrow\rangle_i \uparrow\rangle_j$	$ \uparrow\rangle_i \downarrow\rangle_j$	$ \uparrow\rangle_i \uparrow\rangle_j$
$ \downarrow\rangle_i \downarrow\rangle_j$	1/1			
$ \downarrow\rangle_i \uparrow\rangle_j$		1/4	2/3	
$ \uparrow\rangle_i \downarrow\rangle_j$		3/2	4/1	
$ \uparrow\rangle_i \uparrow\rangle_j$				4/4

TABLE I. Block-diagonal form of the two-site reduced density matrix expressed in terms of generalized correlation functions. Here m/n denotes $\langle \Psi | \mathcal{T}_i^{(m)} \mathcal{T}_j^{(n)} | \Psi \rangle$.

The eigenvalues of the two-site density matrix $\omega^{(\alpha)}$ ($\alpha = 1, \dots, q^2$) can be easily be calculated. Two of the eigenvalues are determined by the 1×1 blocks given by $\langle \mathcal{T}_i^{(1)} \mathcal{T}_j^{(1)} \rangle$ and $\langle \mathcal{T}_i^{(4)} \mathcal{T}_j^{(4)} \rangle$ and can be expressed as

$$\omega_{ij}^{(1)} = \frac{1}{4} - \frac{1}{2} \langle S_i^z \rangle - \frac{1}{2} \langle S_j^z \rangle + \langle S_i^z S_j^z \rangle, \quad (10)$$

$$\omega_{ij}^{(4)} = \frac{1}{4} + \frac{1}{2} \langle S_i^z \rangle + \frac{1}{2} \langle S_j^z \rangle + \langle S_i^z S_j^z \rangle. \quad (11)$$

Here we consider specifically the $S^z \equiv \sum_i S_i^z = 0$ sector for which $\langle S_i^z \rangle = 0$; the expressions above can then be further simplified. Similar calculation leads to

$$\omega_{ij}^{(2,3)} = 1/4 - \langle S_i^z S_j^z \rangle \pm \langle S_i^+ S_j^- \rangle. \quad (12)$$

The entropies s_{ij} , s_i , and s_j as well as the mutual information can be calculated from the eigenvalue spec-

trum of the one- and two-site reduced density matrix. For example, when sites i and j are uncorrelated, both $\langle S_i^z S_j^z \rangle$ and $\langle S_i^+ S_j^- \rangle$ vanish, and $\omega_{ij}^{(\alpha)} = 1/4$ for all α . This means that the two-site subsystem is in a maximally mixed state, and all q^2 states are equally probable. As a consequence, $I_{ij} = 0$ since $s_{ij} = \ln 4$ and $s_i = s_j = \ln 2$.

For the ferromagnetic ground state, an example of an ordered state, $\langle S_i^z S_j^z \rangle = 1/4$, $\langle S_i^z \rangle = \langle S_j^z \rangle = 1/2$, and $\langle S_i^+ S_j^- \rangle = 0$; thus, $\omega_{ij}^{(4)} = 1$ and $\omega_{ij}^{(\alpha)} = 0$ for $\alpha = 1, 2, 3$. Since the two-site subsystem is in a pure state, it is fully separable from the rest of the system. The correlation between sites i and j , as given by the mutual information I_{ij} , is also zero, since $s_i = s_j = 0$.

The spatial behavior of the mutual information can be analyzed as a function of the distance $l = |i - j|$. In general, the eigenvalues depend on the distance l and their decay to zero or a constant value can be analyzed. The decay rate for a given eigenvalue can depend on more than one correlation function. Therefore, in order to determine the exponent of the decay of the eigenvalues in the $l \rightarrow \infty$ limit, one has to analyze all the generalized correlation functions that comprise a particular eigenvalue.

The asymptotic behavior of the mutual information can also be determined in terms of the asymptotic behavior of the generalized correlation functions. When the expectation values of the generalized correlation functions become small for large distance $l = |i - j|$, the von Neumann entropy for two sites, $s_{ij} = -\sum_{\alpha} \omega_{ij}^{(\alpha)} \ln \omega_{ij}^{(\alpha)}$ can be series-expanded using $\ln(1+x) \approx x - \frac{x^2}{2}$, when $x \ll 1$. In order to determine the leading terms in s_{ij} , we keep the second-order terms in the series expansion and obtain to leading order,

$$s_{ij} \approx \ln 4 - 8 \langle S_i^z S_j^z \rangle^2 - 4 \langle S_i^+ S_j^- \rangle^2 \quad (13)$$

for large $l = |i - j|$. Since s_i is a constant, it follows from Eqs. (2) and (13) that I_{ij} decays as the square of the slowest decaying correlation function.

This analysis can be extended to higher spin values and to models with more than one quantum number. For example, for a spin-one model, the two-site density matrix contains 19 different generalized two-site correlation functions. For a spin-1/2 fermionic model, 36 different two-site general correlation functions have to be calculated;^{16,52} they are given explicitly in Ref. 55 but are also summarized in Sec. IV. For fermions with larger numbers of flavors, this number increases significantly. To indicate how this occurs, we summarize the number of nonzero matrix elements in the reduced two-site density matrix, i.e., the number of operator combinations to be calculated, in Table II for the models studied in the present work. Note that the number of non-vanishing independent correlation functions to be calculated can be reduced by taking into account up-down or left-right symmetries.

We note that the procedure outlined above can be ex-

Model	q	N_{ops}
S=1/2 spin	2	6
S=1 spin	3	19
2-flavor fermion	4	36
3-flavor fermion	8	216
4-flavor fermion	16	1296
5-flavor fermion	32	7776

TABLE II. Number of nonzero matrix elements of the two-site reduced density matrix for S -spin bosonic and S -flavor fermion systems with local Hilbert space dimension q .

tended to obtain the n -site reduced density matrix. However, the structure of correlations as well as that of the entanglement becomes much more complicated if more than two sites are involved,⁶¹ and, accordingly, the relevant measures of correlations and their interpretations are not well understood. Nevertheless, the correlation in the respective subsystems can be characterized by generalizations of the two-site mutual information. For example, the three-site correlation can be defined as a Venn-diagram-based three-site generalization⁶² of the two-site mutual information,

$$I_{ijk} = s_i + s_j + s_k - s_{ij} - s_{ik} - s_{jk} + s_{ijk}. \quad (14)$$

The three-site reduced density matrix ρ_{ijk} can be expressed in a straightforward way; Table III gives its definition for the spin-1/2 case.

	$\downarrow\downarrow\downarrow$	$\downarrow\downarrow\uparrow$	$\downarrow\uparrow\downarrow$	$\uparrow\downarrow\downarrow$	$\downarrow\uparrow\uparrow$	$\uparrow\downarrow\uparrow$	$\uparrow\uparrow\downarrow$	$\uparrow\uparrow\uparrow$
$\downarrow\downarrow\downarrow$	1/1/1							
$\downarrow\downarrow\uparrow$		1/1/4	1/2/3	2/1/3				
$\downarrow\uparrow\downarrow$		1/3/2	1/4/1	2/3/1				
$\uparrow\downarrow\downarrow$		3/1/2	3/2/1	4/1/1				
$\downarrow\uparrow\uparrow$					1/4/4	2/3/4	2/4/3	
$\uparrow\downarrow\uparrow$					3/2/4	4/1/4	4/2/3	
$\uparrow\uparrow\downarrow$					3/4/2	4/3/2	4/4/1	
$\uparrow\uparrow\uparrow$								4/4/4

TABLE III. Block-diagonal form of the three-site density matrix expressed in terms of correlation functions. Here $\downarrow\downarrow\downarrow$ denotes the state $|\downarrow\rangle_i|\downarrow\rangle_j|\downarrow\rangle_k$ and $m/n/l$ denotes $\langle\Psi|\mathcal{T}_i^{(m)}\mathcal{T}_j^{(n)}\mathcal{T}_k^{(l)}|\Psi\rangle$.

III. ANISOTROPIC SPIN-1/2 HEISENBERG CHAIN

We consider first the anisotropic spin-1/2 Heisenberg chain where the numerical results can be compared to exactly known behavior. The Hamiltonian has the form

$$H = \sum_i \left[\frac{1}{2}(S_i^+ S_{i+1}^- + S_i^- S_{i+1}^+) + \Delta S_i^z S_{i+1}^z \right] \quad (15)$$

where S_i^+ and S_i^- are the spin raising and lowering operators, respectively, S_i^z is the z component of the spin, and Δ parameterizes the anisotropy. The ground state of the system is critical for $-1 < \Delta \leq 1$, and it has ferromagnetic and antiferromagnetic order for $\Delta \leq -1$ and $\Delta > 1$, respectively.

In order to characterize the behavior, we consider the critical exponents ν_a of the correlation functions $\langle S_i^a S_j^a \rangle \sim |i-j|^{-\nu_a}$ with $a \in \{x, y, z\}$. The values of these critical exponents have a known dependence on Δ .⁶³

$$\nu_x = \nu_y = 1/\nu_z = 1 - \arccos(\Delta)/\pi. \quad (16)$$

As discussed in Sec. II C, the generalized correlation functions $\langle \mathcal{T}_i^{(m)} \mathcal{T}_j^{(n)} \rangle$ can be expressed directly in terms of the spin-spin correlation functions $\langle S_i^z S_j^z \rangle$ and $\langle S_i^+ S_j^- \rangle$, so that the ν_a in Eq. (16) should directly determine the behavior of $\langle \mathcal{T}_i^{(m)} \mathcal{T}_j^{(n)} \rangle$.

The correlation functions depend essentially on the type of intermediate states for which the matrix elements of $\mathcal{T}_i^{(m)}$ and $\mathcal{T}_j^{(n)}$ are finite between these states and the ground state. In conformal field theory, the two-site correlation functions fall into groups characterized by the value of the exponent, which we will denote by ν_{gk} , where k labels the group number. Although the XXZ Heisenberg chain is not conformally invariant, its correlation functions decay with an oscillatory amplitude, and the system has a tower structure in the excitation spectrum. Eq. (16) implies that there will be algebraic decay that falls into two groups in general, $\nu_x = \nu_y$ and $\nu_z = 1/\nu_x$, which coalesce into one group for $\Delta = 1$. In Fig. 2(a), we have plotted the absolute value of the connected part $\langle \mathcal{T}_i^{(m)} \mathcal{T}_j^{(n)} \rangle_C$ of the two independent generalized two-site correlation functions used to construct the two-site reduced density matrix (see Table I) as well as I_{ij} itself. Correlations measured in the bulk are plotted as a function of j for $i = N/4$ for $\Delta = 1$ and various system sizes on a log-log scale. For the SU(2) symmetric case, $\Delta = 1$, we find that both independent generalized correlation functions scale to zero algebraically as $l \rightarrow \infty$ with an exponent $\nu_{g1} = 0.95(3)$, i.e., they do, in fact, form a single group. The mutual information $I_{N/4, N/4+l}$ also decays to zero algebraically, $I_{N/4, N/4+l} \sim l^{\nu_I}$, but with a different exponent, $\nu_I = 1.97(3) \simeq 2 \times \nu_{g1}$. For the isotropic case $\langle S_i^+ S_j^- \rangle = 2 \langle S_i^z S_j^z \rangle$, the four eigenvalues derived from Eqs. (11,12) are $\omega_{ij}^{(1,2,4)} = 1/4 + \langle S_i^z S_j^z \rangle$, $\omega_{ij}^{(3)} = 1/4 - 3 \langle S_i^z S_j^z \rangle$, and $s_{ij} = \ln 4 - 24 \langle S_i^z S_j^z \rangle^2$, so the exact value of $\nu_I = 2$.

For $\Delta \neq 1$, we summarize the content and behavior of the two groups of correlation functions, corresponding to longitudinal and transverse correlations, in Table IV for $\Delta = 0.5$. We obtain $\nu_{g1} = 1.48(3)$ (exact value: $\nu_z = 3/2$), $\nu_{g2} = 0.69(4)$ (exact value $\nu_x = \nu_y = 2/3$), and $\nu_I = 1.39(5)$ (exact value: $\nu_I = 2 \times \nu_{g1} = 4/3$). Thus, here we also find that the mutual information decays twice as fast as the slowest decaying correlation

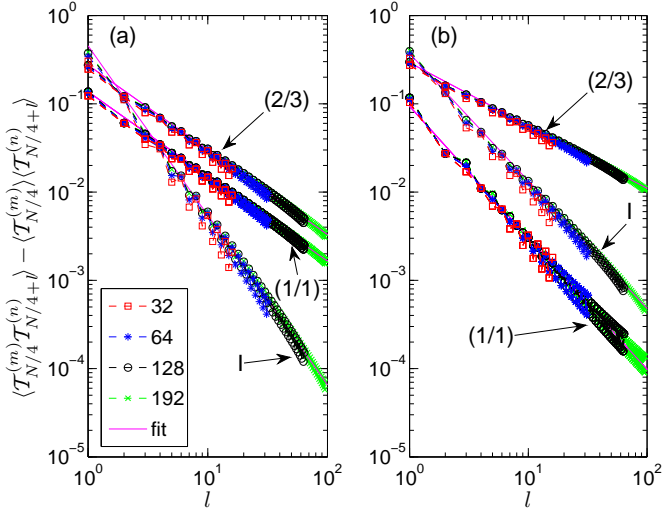


FIG. 2. (Color online) Decay of the connected part $\langle \mathcal{T}_{N/4}^{(m)} \mathcal{T}_{N/4+l}^{(n)} \rangle_C$ of the various two-site general correlation functions used to construct the two-site density matrix and the two-site mutual information $I_{N/4, N/4+l}$ as a function of distance l for various system sizes on a log-log scale for (a) $\Delta = 1$ and (b) $\Delta = 0.5$. The solid lines show linear fits used to obtain decay exponents for $(m/n) = (2/3)$, $(1/1)$, and $(4/4)$, and for $I_{N/4, N/4+l}$.

function, as can be seen explicitly in Fig. 2(b). For a purely XX interaction, $\Delta = 0$, we obtain $\nu_{g1} = 0.52(5)$ for $\langle \mathcal{T}_1^{(2)} \mathcal{T}_l^{(3)} \rangle$ (exact value: $\nu_x = \nu_y = 0.5$), while $\langle \mathcal{T}_1^{(1)} \mathcal{T}_l^{(1)} \rangle$, $\langle \mathcal{T}_1^{(1)} \mathcal{T}_l^{(4)} \rangle$, $\langle \mathcal{T}_1^{(4)} \mathcal{T}_l^{(1)} \rangle$, and $\langle \mathcal{T}_1^{(4)} \mathcal{T}_l^{(4)} \rangle$ decay with an exponent $\nu_{g2} = 2.15(8)$ (exact value: $\nu_z = 2$). The mutual information decays with the exponent $\nu_I = 1.07(3) \simeq 2 \times \nu_{g1}$.

Note that in order to obtain more accurate values for the critical exponents, we would have to carry out an accurate finite-size scaling, probably including non-leading effects such as logarithmic corrections.⁶⁴ When the U(1) symmetry is broken, for example, by switching on a magnetic field, $\langle \mathcal{T}^{(1)} \mathcal{T}^{(1)} \rangle \neq \langle \mathcal{T}^{(4)} \mathcal{T}^{(4)} \rangle$ and $\langle \mathcal{T}^{(1)} \mathcal{T}^{(4)} \rangle \neq \langle \mathcal{T}^{(4)} \mathcal{T}^{(1)} \rangle$. In this case, the correlation functions break up completely into different groups. In higher spin sectors, we find the same relationship, but additional oscillations appear in the decay of the correlation functions, and $\langle S_i^z S_j^z \rangle$ scales to a finite value due to the finite value of $S_{\text{tot}}^z = \sum_i S_i^z$.

IV. SU(n) HUBBARD MODEL

In this section, we apply our method to the SU(n) symmetric Hubbard model for $n = 2, 3, 4$, and 5 for commensurate fillings $f = p/q$, where p and q are relatively

Group-1 (algebraic), $\nu_{g1} = 0.69(4)$			
Operator combination denoted as (m/n)	Second quantized form $\mathcal{T}_i^{(m)} \mathcal{T}_j^{(n)}$	ΔS	G
$(2/3)$	$S_i^- S_j^+$	-1	G^{xx}, G^{yy}
$(3/2)$	$S_i^+ S_j^-$	1	G^{xx}, G^{yy}
Group-2 (algebraic), $\nu_{g2} = -1.48(3)$			
$(1/1)$	$(-S^z + \frac{1}{2}\mathbb{1})_i (-S^z + \frac{1}{2}\mathbb{1})_j$	0	G^{zz}
$(1/4)$	$(-S^z + \frac{1}{2}\mathbb{1})_i (S^z + \frac{1}{2}\mathbb{1})_j$	0	G^{zz}
$(4/1)$	$(S^z + \frac{1}{2}\mathbb{1})_i (-S^z + \frac{1}{2}\mathbb{1})_j$	0	G^{zz}
$(4/4)$	$(S^z + \frac{1}{2}\mathbb{1})_i (S^z + \frac{1}{2}\mathbb{1})_j$	0	G^{zz}
Mutual information (algebraic), $\nu_I = -1.39(5)$			

TABLE IV. Characterization of the two-site correlation functions based on their decay type and the value of their exponent for the spin-1/2 anisotropic Heisenberg chain at $\Delta = 0.5$ with $N = 128$ sites. Here ΔS shows how $\mathcal{T}_i^{(m)}$ changes the spin quantum number. The corresponding conventional correlation functions as given in Eq. (9) are indicated by G . Operator combinations in group 1 correspond to transverse components and in group 2 to the longitudinal component of the spin correlations. The exact critical exponents are $\nu_x = \nu_y = 2/3$ and $\nu_z = 3/2$.

prime. The SU(n) Hubbard model has the Hamiltonian

$$\mathcal{H} = -t \sum_{i=1}^N \sum_{\sigma=1}^n (c_{i,\sigma}^\dagger c_{i+1,\sigma} + c_{i+1,\sigma}^\dagger c_{i,\sigma}) + \frac{U}{2} \sum_{i=1}^N \sum_{\substack{\sigma,\sigma'=1 \\ \sigma \neq \sigma'}}^n n_{i,\sigma} n_{i,\sigma'}, \quad (17)$$

where N is the number of sites in the chain. The operator $c_{i,\sigma}^\dagger$ ($c_{i,\sigma}$) creates (annihilates) an electron at site i with spin σ , where the spin index is allowed to take on n different values. Here $n_{i,\sigma}$ denotes the particle-number operator, t the hopping integral between nearest-neighbor sites, and U the strength of the on-site Coulomb repulsion. For consistency, the spin (or, for $n > 2$, flavor) index of the operators will be indicated by a subscript index running from 1 to n , even for the SU(2) case. In what follows, we will take t as the unit of energy.

By studying the length-dependence of the entropy of finite blocks of long chains, some of us showed in a previous work⁶⁵ that the system has drastically different behavior depending on whether $q > n$, $q = n$, or $q < n$. In addition, by taking the Fourier transform of the oscillatory behavior of the block entropy,²¹ we were able to determine the position of soft modes in the excitation spectrum when the model is critical and the spatial inhomogeneity of the ground state when the system is gapped.⁶⁶

When $q > n$, the umklapp processes are irrelevant, and the model is equivalent to an n -component Luttinger liquid with central charge $c = n$. When $q = n$, the charge and spin modes are decoupled, and the umklapp processes open a charge gap for finite $U_c > 0$, while the spin modes remain gapless and the central charge $c =$

$n - 1$. The value of U_c is still a subject of debate,^{65,67,68} but it is known that the translational symmetry is not broken in the ground state for any n .

On the other hand, when $q < n$, the charge and spin modes are coupled, the umklapp processes open gaps in all excitation branches, and a spatially non-uniform ground state develops. Bond-ordered dimerized, trimerized, or tetramerized phases can be found as the filling is varied. These known results are summarized in Table V, and a schematic plot of the spatial inhomogeneity of the ground state determined using dimerization entropy is shown in Fig. 3 for various fillings and n values.

	n	c	phase	k^*
$q = n$	any n	$n - 1$	COS($n - 1$)	$2\pi p/n$
$q < n$	$n \neq 2$	-	COS0	$2\pi p/q$
$q > n$	any n	n	C1S($n - 1$)	$2\pi p/q$

TABLE V. Central charge c and type of phase, as characterized by the number of soft modes in the charge and spin sectors (CxSy), for the p/q -filled $SU(n)$ Hubbard model.

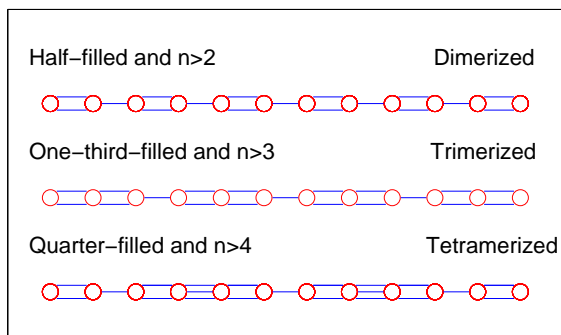


FIG. 3. (Color online) Depiction of the spatial inhomogeneity of the ground state of the $SU(n)$ Hubbard model in the thermodynamic limit for various fillings and $q < n$. The strength of the bond is indicated by the number of lines connecting nearest-neighbor sites.

This picture was obtained by calculating the spatial variation of the two-site entropies of neighboring sites along the chain. In this paper we will get a more quantitative description of the dimerized, trimerized, and quadrimerized phases by calculating the spatial entanglement maps of the two-site mutual information. Extracting such spatial entanglement information and identifying the underlying physical processes will be the subject of the rest of this section.

A. The half-filled $SU(2)$ Hubbard model

The $SU(2)$ Hubbard model is a free fermion model for $U = 0$ and is thus trivially conformally invariant. Therefore, the results discussed in the previous section hold in this case. For finite U and away from half filling, the

model is also conformally invariant, whereas for finite U at half filling, the model is not conformally invariant. Our procedure, however, also applies to non-conformally invariant models, as will be shown below.

For convenience, we use the standard notation \uparrow and \downarrow for the $\sigma = \{1, 2\}$ spin states. For a spin-1/2 fermionic model, single-electron basis states can be empty, occupied with a single spin-down or spin-up electron, or doubly occupied. These states we denote as $|-\rangle$, $|\downarrow\rangle$, $|\uparrow\rangle$, and $|\uparrow\downarrow\rangle$, respectively. Since the local basis is four-dimensional, 16 possible transition operators $\mathcal{T}_i^{(m)}$, as displayed in Table VI, arise. They can be written explicitly in terms of local fermion creation $c_{i\sigma}^\dagger$, annihilation $c_{i\sigma}$ and density $n_{i\sigma}$ operators as

$$\begin{aligned}
 \mathcal{T}^{(1)} &= (\mathbb{1} - n_\uparrow)(\mathbb{1} - n_\downarrow), & \mathcal{T}^{(2)} &= (\mathbb{1} - n_\uparrow)c_\downarrow, \\
 \mathcal{T}^{(3)} &= c_\uparrow(\mathbb{1} - n_\downarrow), & \mathcal{T}^{(4)} &= -c_\uparrow c_\downarrow, \\
 \mathcal{T}^{(5)} &= (\mathbb{1} - n_\uparrow)c_\downarrow^\dagger, & \mathcal{T}^{(6)} &= (\mathbb{1} - n_\uparrow)n_\downarrow, \\
 \mathcal{T}^{(7)} &= -c_\uparrow c_\downarrow^\dagger, & \mathcal{T}^{(8)} &= c_\uparrow n_\downarrow, \\
 \mathcal{T}^{(9)} &= c_\uparrow^\dagger(\mathbb{1} - n_\downarrow), & \mathcal{T}^{(10)} &= c_\uparrow^\dagger c_\downarrow, \\
 \mathcal{T}^{(11)} &= n_\uparrow(\mathbb{1} - n_\downarrow), & \mathcal{T}^{(12)} &= -n_\uparrow c_\downarrow, \\
 \mathcal{T}^{(13)} &= c_\uparrow^\dagger c_\downarrow^\dagger, & \mathcal{T}^{(14)} &= c_\uparrow^\dagger n_\downarrow, \\
 \mathcal{T}^{(15)} &= -n_\uparrow c_\downarrow^\dagger, & \mathcal{T}^{(16)} &= n_\uparrow n_\downarrow.
 \end{aligned} \tag{18}$$

Recalling that in this case 36 independent correlation functions can be constructed (see Table II), we will now relate them to ρ_{ij} . Following the procedure outlined in Sec. II A, the non-vanishing matrix elements of the two-site density matrix ρ_{ij} are given in Table VII. Note that the two-site density matrix is block-diagonal in the particle number N_c and in the z component of the spin S_z . The block-diagonal structure is evident, and the values of m and n appropriate for each matrix element are displayed.

	$ -\rangle_i$	$ \downarrow\rangle_i$	$ \uparrow\rangle_i$	$ \uparrow\downarrow\rangle_i$
$ -\rangle_i$	$\mathcal{T}_i^{(1)}$	$\mathcal{T}_i^{(2)}$	$\mathcal{T}_i^{(3)}$	$\mathcal{T}_i^{(4)}$
$ \downarrow\rangle_i$	$\mathcal{T}_i^{(5)}$	$\mathcal{T}_i^{(6)}$	$\mathcal{T}_i^{(7)}$	$\mathcal{T}_i^{(8)}$
$ \uparrow\rangle_i$	$\mathcal{T}_i^{(9)}$	$\mathcal{T}_i^{(10)}$	$\mathcal{T}_i^{(11)}$	$\mathcal{T}_i^{(12)}$
$ \uparrow\downarrow\rangle_i$	$\mathcal{T}_i^{(13)}$	$\mathcal{T}_i^{(14)}$	$\mathcal{T}_i^{(15)}$	$\mathcal{T}_i^{(16)}$

TABLE VI. Single-site operators describing transitions between single-site basis states for a $S = 1/2$ spin system.

We analyze the decay properties of the various generalized correlation functions that appear in the operator decomposition of the reduced two-site density matrix, as given in Eq. (18) and Table VII, and the two-site mutual information. The exact critical exponents of conventional correlation functions, which have the form $G_{i,i+l} = \langle A_i A_{i+l}^\dagger \rangle \sim l^{-\nu_G}$, where A is a single-site spin, density, fermion-creation, or pair-creation operator (see Table VIII), are known from the effective conformal field

$\rho_{i,j}$	$N_c=0, S^z=0$	$N_c=1, S^z=-\frac{1}{2}$		$N_c=1, S^z=\frac{1}{2}$		$N_c=2, S^z=-1$	$N_c=2, S^z=0$				$N_c=2, S^z=1$	$N_c=3, S^z=-\frac{1}{2}$		$N_c=3, S^z=\frac{1}{2}$		$N_c=4, S^z=0$
	--	-↓	↓-	-↑	↑-	↓↓	-↑↓	↓↑	↑↓	↑-	↑↑	↓↑	↑↓	↑↑	↑↑	↑↑
--	1/1															
-↓		1/6	2/5													
↓-		5/2	6/1													
-↑				1/11	3/9											
↑-				9/3	1/11											
↓↓						6/6										
-↑↓							1/16	2/15	3/14	4/13						
↓↑							5/12	6/11	7/10	8/9						
↑↓							9/8	10/7	11/6	12/5						
↑-							13/4	14/3	15/2	16/1						
↑↑											11/11					
↓↑												6/16	8/14			
↑↓												14/8	16/6			
↑↑														11/16	12/15	
↑↑														15/12	16/11	
↑↑																16/16

TABLE VII. The two-site reduced density matrix ρ_{ij} for SU(2) fermions expressed in terms of single-site operators, $\mathcal{T}_i^{(m)}$ with $m = 1 \cdots 16$. For easier readability only the upper indices of the operators are shown; thus, m/n denotes $\langle \mathcal{T}_i^{(m)} \mathcal{T}_j^{(n)} \rangle$. Here N_c and S^z are the particle-number and z spin component quantum numbers of the two sites.

Half-filled case		
G	$U = 0$	$U > 0$
$G_{c_\sigma^\dagger c_\sigma} = \langle c_\sigma^\dagger c_\sigma \rangle$	$\nu = 1$	-
$G_{nn} = \langle n n \rangle$	$\nu = 2$	1
$G^{zz} = \langle S^z S^z \rangle$	$\nu = 2$	1
$G^{+-} = \langle S^+ S^- \rangle$	$\nu = 2$	1
$G_p^{(0)} = \langle c_1^\dagger c_2^\dagger c_2 c_1 \rangle$	$\nu = 2$	-
Non half-filled case		
G	$U = 0$	$U \gg W$
$G_{c_\sigma^\dagger c_\sigma} = \langle c_\sigma^\dagger c_\sigma \rangle$	$\nu = 1$	9/8
$G_{nn} = \langle n n \rangle$	$\nu = 2$	3/2
$G^{zz} = \langle S^z S^z \rangle$	$\nu = 2$	3/2
$G^{+-} = \langle S^+ S^- \rangle$	$\nu = 2$	3/2
$G_p^{(0)} = \langle c_1^\dagger c_2^\dagger c_2 c_1 \rangle$	$\nu = 2$	5/2

TABLE VIII. Conventional correlation functions and corresponding exact values of the critical exponents, where $n = n_1 + n_2$, $S^z = (n_1 - n_2)/2$ and $S^\pm = c_\sigma^\dagger c_{\sigma'}$ with $\sigma \in \{\downarrow, \uparrow\} \equiv \{\downarrow, \uparrow\}$ and $W = 4t$ is the bandwidth.

theory and are related to the behavior of finite-size corrections to the ground state.⁶⁹⁻⁷² They are determined by the operator content of A , namely, by the number of creation and annihilation operators for up- or down-spin particles on the two branches (left and right) of the dispersion relation. The exponents depend in a relatively simple manner on four parameters, i.e., on how the operator A changes the number of electrons, ΔN_c , the spin, ΔS^z , and on the value of charge current J_c and spin current J_s . In general, the exponents depend on U , and are known exactly in the limiting cases. They are summarized in Table VIII for both the half-filled and the non-half-filled systems. At half filling, a metal-insulator transition takes place at $U = 0$, leading to different be-

havior for $U = 0$ and $U > 0$. For the non-half-filled case, the prefactor of the leading term, which determines the critical exponent of the correlation function, may vanish in the $U \rightarrow \infty$ limit.⁶⁹ Therefore, the $U = \infty$ case must be treated separately. For example, for finite but large U , $\nu_{G_{nn}} = 3/2$, whereas $\nu_{G_{nn}} = 2$ for $U = \infty$.

We can express the conventional correlation functions as linear combinations of the generalized correlation functions. For example, using the definitions of single-site transition operators as given in Eq. (18) and noting that

$$c_\downarrow^\dagger = c_\downarrow(\mathbb{1} - n_\uparrow) + c_\downarrow n_\uparrow = \mathcal{T}^{(5)} - \mathcal{T}^{(15)}, \quad (19)$$

$$c_\uparrow^\dagger = c_\uparrow(\mathbb{1} - n_\downarrow) + c_\uparrow n_\downarrow = \mathcal{T}^{(9)} + \mathcal{T}^{(14)}, \quad (20)$$

$$c_\downarrow = c_\downarrow(\mathbb{1} - n_\uparrow) + c_\downarrow n_\uparrow = \mathcal{T}^{(2)} - \mathcal{T}^{(12)}, \quad (21)$$

$$c_\uparrow = c_\uparrow(\mathbb{1} - n_\downarrow) + c_\uparrow n_\downarrow = \mathcal{T}^{(3)} + \mathcal{T}^{(8)}, \quad (22)$$

$$n_\downarrow = n_\downarrow(\mathbb{1} - n_\uparrow) + n_\downarrow n_\uparrow = \mathcal{T}^{(6)} + \mathcal{T}^{(16)}, \quad (23)$$

$$n_\uparrow = (\mathbb{1} - n_\downarrow)n_\uparrow + n_\downarrow n_\uparrow = \mathcal{T}^{(11)} + \mathcal{T}^{(16)}, \quad (24)$$

$$\begin{aligned} S^z &= \frac{1}{2}(n_\uparrow - n_\downarrow) = \frac{1}{2}(n_\uparrow(\mathbb{1} - n_\downarrow) - n_\downarrow(\mathbb{1} - n_\uparrow)) \\ &= \frac{1}{2}(\mathcal{T}^{(11)} - \mathcal{T}^{(6)}), \end{aligned} \quad (25)$$

the conventional correlation functions can be written as

$$\begin{aligned}
G_{nn} &= \langle \mathcal{T}_i^{(6)} \mathcal{T}_j^{(6)} \rangle + \langle \mathcal{T}_i^{(6)} \mathcal{T}_j^{(11)} \rangle + 2 \langle \mathcal{T}_i^{(6)} \mathcal{T}_j^{(16)} \rangle \\
&+ \langle \mathcal{T}_i^{(11)} \mathcal{T}_j^{(6)} \rangle + \langle \mathcal{T}_i^{(11)} \mathcal{T}_j^{(11)} \rangle + 2 \langle \mathcal{T}_i^{(11)} \mathcal{T}_j^{(16)} \rangle \\
&+ 2 \langle \mathcal{T}_i^{(16)} \mathcal{T}_j^{(6)} \rangle + 2 \langle \mathcal{T}_i^{(16)} \mathcal{T}_j^{(11)} \rangle + 4 \langle \mathcal{T}_i^{(16)} \mathcal{T}_j^{(16)} \rangle, \\
G^{zz} &= \frac{1}{4} (\langle \mathcal{T}_i^{(11)} \mathcal{T}_j^{(11)} \rangle + \langle \mathcal{T}_i^{(6)} \mathcal{T}_j^{(6)} \rangle) \\
&- \frac{1}{4} (\langle \mathcal{T}_i^{(6)} \mathcal{T}_j^{(11)} \rangle + \langle \mathcal{T}_i^{(11)} \mathcal{T}_j^{(6)} \rangle), \tag{26}
\end{aligned}$$

$$G^{+-} = \langle \mathcal{T}_i^{(7)} \mathcal{T}_j^{(10)} \rangle, \tag{27}$$

$$\begin{aligned}
G_{c_\uparrow^\dagger c_\downarrow} &= \langle \mathcal{T}_i^{(5)} \mathcal{T}_j^{(2)} \rangle - \langle \mathcal{T}_i^{(5)} \mathcal{T}_j^{(12)} \rangle \\
&- \langle \mathcal{T}_i^{(15)} \mathcal{T}_j^{(2)} \rangle + \langle \mathcal{T}_i^{(15)} \mathcal{T}_j^{(12)} \rangle, \tag{28}
\end{aligned}$$

$$\begin{aligned}
G_{c_\uparrow^\dagger c_\uparrow} &= \langle \mathcal{T}_i^{(9)} \mathcal{T}_j^{(3)} \rangle + \langle \mathcal{T}_i^{(9)} \mathcal{T}_j^{(8)} \rangle \\
&+ \langle \mathcal{T}_i^{(14)} \mathcal{T}_j^{(3)} \rangle + \langle \mathcal{T}_i^{(14)} \mathcal{T}_j^{(8)} \rangle, \tag{29}
\end{aligned}$$

$$G_p^{(0)} = \langle \mathcal{T}_i^{(13)} \mathcal{T}_j^{(4)} \rangle. \tag{30}$$

For $U = 0$, all generalized correlation functions and thus the mutual information decay algebraically due to soft modes at $k = 0$ and $k = 2k_F$ in both the spin and charge sectors. These soft modes lead to a $2k_F$ oscillation in the leading terms. Grouping the operators according to their decay type and increasing value of the exponent (see Table IX), we identify three groups. The correlation functions with the slowest algebraic decay are those in group 1. They are composed of operators describing single-particle transfer processes weighted by the occupation number of the spin-up and down-particle in various ways. Specifically, these generalized correlation functions have the form $\langle A_i B_i A_j^\dagger B_j' \rangle$, where, for example, $A \equiv c_\uparrow$, and B and $B' \in \{n_\uparrow, 1 - n_\uparrow\}$. The corresponding single-site transition operators change the number of electrons by $\Delta N_c = \pm 1$ and the spin by $\Delta S^z = \pm 1/2$, and we obtain the exponent $\nu_{g1} \simeq 0.98(4)$. Operators in the generalized correlation functions falling into group 2 describe density-like correlations, $\Delta N_c = 0$, $\Delta S^z = 0$, and decay algebraically with an exponent $\nu_{g2} \simeq 3.89(6)$. The generalized correlation functions have the form $\langle A_i B_i A_j' B_j' \rangle$ with $A_i, A_j', B_i, B_j' \in \{n_\uparrow, n_\downarrow, (1 - n_\uparrow), (1 - n_\downarrow)\}$, and the corresponding single-site transition operators are related to basis states with odd numbers of particles. Operators falling into group 3 describe spin-, density-, and pair-like correlations $\Delta N_c \in \{0, \pm 2\}$, $\Delta S^z \in \{\pm 1, 0\}$, and decay algebraically with an exponent $\nu_{g3} \simeq 1.93(5)$. The corresponding single-site transition operators are related to basis states with even numbers of particles.

We now consider the physical correlation functions, in particular, the equal-time single- and two-particle Green functions. According to Eq. (26), G_{nn} can be expressed as a linear combination of generalized correlation functions from group 2 and group 3; therefore, the smallest ν of these two groups determine $\nu_{G_{nn}} \simeq 1.92(5)$, which is in agreement with the analytic result given in Table VIII. According to Eqs. (27) and (28), G^{zz} and

(m/n)	Second quantized form $A_i B_j$	ΔN_c	ΔS^z	G
Group-1(algebraic) $\nu_{g1} = 0.98(4)$				
(12/15)	$[n_\uparrow c_\downarrow]_i [n_\uparrow c_\uparrow^\dagger]_j$	-1	0.5	$G_{c_\uparrow c_\uparrow^\dagger}$
(2/15)	$[(\mathbb{1} - n_\uparrow) c_\downarrow]_i [-n_\uparrow c_\uparrow^\dagger]_j$	-1	0.5	$G_{c_\uparrow c_\uparrow^\dagger}$
(2/5)	$[(\mathbb{1} - n_\uparrow) c_\downarrow]_i [(\mathbb{1} - n_\uparrow) c_\uparrow^\dagger]_j$	-1	0.5	$G_{c_\uparrow c_\uparrow^\dagger}$
(3/14)	$[c_\uparrow (\mathbb{1} - n_\downarrow)]_i [c_\uparrow^\dagger n_\downarrow]_j$	-1	-0.5	$G_{c_\uparrow c_\uparrow^\dagger}$
(3/9)	$[c_\uparrow (\mathbb{1} - n_\downarrow)]_i [c_\uparrow^\dagger (\mathbb{1} - n_\downarrow)]_j$	-1	-0.5	$G_{c_\uparrow c_\uparrow^\dagger}$
(5/12)	$[(\mathbb{1} - n_\uparrow) c_\downarrow^\dagger]_i [-n_\uparrow c_\downarrow]_j$	1	-0.5	$G_{c_\uparrow^\dagger c_\downarrow}$
(8/14)	$[c_\uparrow n_\downarrow]_i [c_\uparrow^\dagger n_\downarrow]_j$	-1	-0.5	$G_{c_\uparrow^\dagger c_\downarrow}$
(8/9)	$[c_\uparrow n_\downarrow]_i [c_\uparrow^\dagger (\mathbb{1} - n_\downarrow)]_j$	-1	-0.5	$G_{c_\uparrow^\dagger c_\downarrow}$
Group-2(algebraic) $\nu_{g2} = 1.92(5)$				
(11/11)	$[n_\uparrow (\mathbb{1} - n_\downarrow)]_i [n_\uparrow (\mathbb{1} - n_\downarrow)]_j$	0	0	$G_{nn}, G_{\sigma\sigma}^z$
(16/16)	$[n_\uparrow n_\downarrow]_i [n_\uparrow n_\downarrow]_j$	0	0	G_{nn}
(1/16)	$[(\mathbb{1} - n_\uparrow) (\mathbb{1} - n_\downarrow)]_i [n_\uparrow n_\downarrow]_j$	0	0	
(1/1)	$[(\mathbb{1} - n_\uparrow) (\mathbb{1} - n_\downarrow)]_i [(\mathbb{1} - n_\uparrow) (\mathbb{1} - n_\downarrow)]_j$	0	0	
(6/11)	$[(\mathbb{1} - n_\uparrow) n_\downarrow]_i [n_\uparrow (\mathbb{1} - n_\downarrow)]_j$	0	0	$G_{nn}, G_{\sigma\sigma}^z$
(6/6)	$[(\mathbb{1} - n_\uparrow) n_\downarrow]_i [(\mathbb{1} - n_\uparrow) n_\downarrow]_j$	0	0	$G_{nn}, G_{\sigma\sigma}^z$
(4/13)	$[-c_\uparrow c_\downarrow]_i [c_\uparrow^\dagger c_\downarrow^\dagger]_j$	-2	0	$G_p^{(0)}$
(7/10)	$[c_\uparrow c_\downarrow^\dagger]_i [-c_\uparrow^\dagger c_\downarrow]_j$	0	-1	G^{+-}
Group-3(algebraic) $\nu_{g3} = 3.89(6)$				
(11/16)	$[n_\uparrow (\mathbb{1} - n_\downarrow)]_i [n_\uparrow n_\downarrow]_j$	0	0	G_{nn}
(1/11)	$[(\mathbb{1} - n_\uparrow) (\mathbb{1} - n_\downarrow)]_i [n_\uparrow (\mathbb{1} - n_\downarrow)]_j$	0	0	
(1/6)	$[(\mathbb{1} - n_\uparrow) (\mathbb{1} - n_\downarrow)]_i [(\mathbb{1} - n_\uparrow) n_\downarrow]_j$	0	0	
(6/16)	$[(\mathbb{1} - n_\uparrow) n_\downarrow]_i [n_\uparrow n_\downarrow]_j$	0	0	G_{nn}
Mutual information $\nu_I = 1.95(4)$				

TABLE IX. Similar to Table IV but for the half-filled SU(2) Hubbard model at $U = 0$. Generalized correlation functions $\langle \mathcal{T}_i^{(m)} \mathcal{T}_j^{(n)} \rangle$ are denoted as (m/n) , and only the $m \leq n$ components are shown. Here ΔN_c and ΔS indicate how $\mathcal{T}_i^{(m)}$ changes the charge and spin quantum numbers, respectively. The corresponding conventional correlation functions, G , are listed in the last column.

G^{+-} are composed of generalized correlation functions from group 3 only; we obtain $\nu_{G^{+-}} = \nu_{G_{xy}} \simeq 1.92(5)$, which is also consistent with the analytic result given in Table VIII. According to Eq. (29), $G_{c_\uparrow^\dagger c_\sigma}$ is composed of generalized correlation functions from group 1 only; we obtain $\nu_{c_\uparrow^\dagger c_\sigma} \simeq 0.98(4)$, reproducing the analytic result given in Table VIII. According to Eq. (30), $G_p^{(0)}$ is composed of generalized correlation functions from group 3 only; we obtain $\nu_{G_p^{(0)}} = 1.92(6)$, in agreement with the analytic result given in Table VIII. We have again confirmed that the mutual information decays with the exponent $\nu_I = 1.95(4)$, which decays twice as fast as the most slowly decaying correlation function, which in this case corresponds to one-particle transfer processes. This means that the quasi-long-range entanglement in the metallic case is due to one-particle-like hopping, as expected.

For $U = 10$, it is known from the analytic picture that the charge modes are gapped, while the spin modes are gapless. Thus, the correlation functions that couple to the charge mode are expected to decay exponentially, while those that couple to the spin mode are expected to decay algebraically. Classifying the correla-

tion functions according to their type of decay and the value of the correlation length or the exponents as described above, we find two groups of exponentially decaying and two groups of algebraically decaying correlation functions, as summarized in Table X. We find that

Group-1(algebraic), $\nu_{g1} = 0.98(3)$
(7/10), (10/7), (6/11), (11/6), (6/6), (11/11)
Group-2(algebraic), $\nu_{g2} = 3.78(3)$
(11/16), (16/11), (1/11), (11/1), (1/16), (16/1), (6/16), (16/6), (1/6), (6/1), (1/1), (16/16)
Group-3(exponential), $\xi_{g3} = 1.07(2)$
(12/15), (15/12), (5/12), (12/5), (3/14), (14/3), (8/14), (14/8), (2/15), (15/2), (2/5), (5/2), (3/9), (9/3), (8/9), (9/8)
Group-4(exponential), $\xi_{g4} = 0.51(3)$
(4/13), (13/4)
Mutual information(algebraic), $\nu_I = 2.08(5)$

TABLE X. Similar to Table IV but for the half-filled SU(2) Hubbard model at $U = 10$. The corresponding single-site transition operators are summarized in Eq. (18). The generalized correlation functions $\langle \mathcal{T}_i^{(m)} \mathcal{T}_j^{(n)} \rangle$ are denoted as (m/n) .

the mutual information again decays twice as fast as the slowest algebraically decaying correlation functions; we obtain an exponent $\nu_I = 1.95(5) \simeq 2 \times 0.98(3)$. The most slowly decaying correlation functions ($\nu_{g1} = 0.98(3)$) are in group 1 and correspond to spin-flip excitations, $\Delta N_c = 0, \Delta S^z \in \{\pm 1, 0\}$, as is to be expected from the spin-density-like nature of the ground state. The one- and two-particle hoppings (groups 3 and 4) decay exponentially, and we find that the decay length of the

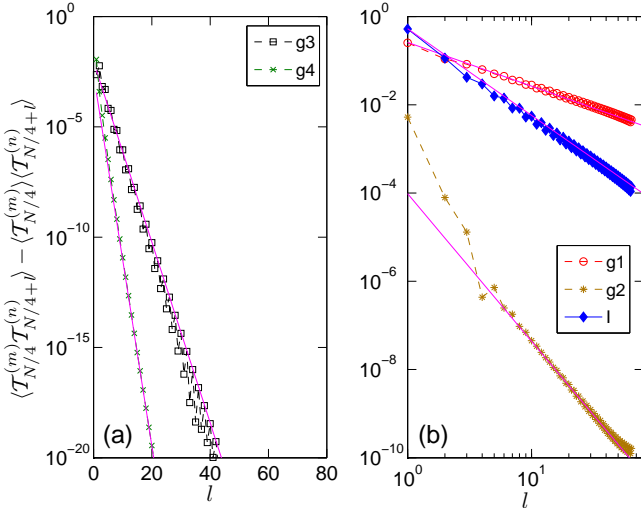


FIG. 4. (Color online) Correlation functions measured relative to the middle of the chain for $U = 10$, with (a) the two groups of exponentially decaying functions plotted on a semi-logarithmic scale and (b) the two groups of algebraically decaying correlation functions plotted on a log-log scale, both as a function of distance l . The straight lines are the results of our fits.

two-particle hopping is twice of that of the single-particle hopping. The reason for this behavior is that the two-particle gap is twice as large as the one-particle gap in the thermodynamic limit, as is shown in Fig. 5(b). Note that the relation $\Delta_{\text{pair}}(N) = 2 \times \Delta_{\text{band}}(N)$ holds for any N at $U = 0$, while this becomes true only in the thermodynamic limit for finite U (Figs. 5(a),(b)).

By carrying out a similar analysis for the quarter-filled case at $U = 10$, we obtain the results displayed in Table XI. The generalized correlation functions fall into

Group-1(algebraic), $\nu_{g1} = 1.12(3)$
(12/15), (15/12), (5/12), (12/5), (3/14), (14/3), (8/14), (14/8), (2/15), (15/2), (8/9), (9/8), (2/5), (5/2), (3/9), (9/3)
Group-2(algebraic), $\nu_{g2} = 1.48(4)$
(7/10), (10/7), (1/11), (11/1), (6/11), (11/6), (1/6), (6/1), (1/1), (6/6), (11/11)
Group-3(algebraic), $\nu_{g3} = 2.47(4)$
(11/16), (16/11), (1/16), (16/1), (6/16), (16/6), (16/16), (4/13), (13/4)
Mutual information(algebraic), $\nu_I = 2.19$

TABLE XI. Similar to Table IV but for the quarter-filled SU(2) Hubbard model at $U = 10$. The corresponding single-site transition operators are summarized in Eq. (18). The generalized correlation functions $\langle \mathcal{T}_i^{(m)} \mathcal{T}_j^{(n)} \rangle$ are denoted as (m/n) .

three groups with exponents $\nu_{g1} = 1.12(3)$, $\nu_{g2} = 1.48(4)$, and $\nu_{g3} = 2.47(4)$. Applying Eqs. (26)–(30), we obtain the corresponding exponents of the conventional correlation functions, $\nu_{G_{c_{\uparrow}c_{\sigma}}^{\dagger}c_{\sigma}} = 1.12(3)$, $\nu_{G_{nn}} = \nu_{G^{zz}} = \nu_{G^{+-}} = 1.48(4)$, and $\nu_{G_p^{(0)}} \nu \simeq 2.47(4)$, again in agreement with the analytic results given in Table VIII. The mutual information decays algebraically with an exponent $\nu_I = 2.19(4)$, indicating that the long-range entanglement is due to the one-particle hopping term here as well.

B. SU(n) Hubbard model with $n > 2$

Next we consider the SU(n) Hubbard model with $n > 2$ at half filling, $f = 1/2$, for large Coulomb interaction, $U = 10$. It has been shown using bosonization that, in this case, the ground state is dimerized for even values of n .⁷³ The same scenario has also been shown numerically to occur for odd n values.⁶⁶ For $n = 3$ and $q < n$, only the half-filled case occurs; therefore, we investigate the entanglement pattern for the $n = 4$ and $n = 5$ cases only. The results for a finite chain of length $N = 24$ for $n = 4$ are displayed in Fig. 6(a), finite-size scaling of the leading entangled bonds in Fig. 6(b), and the resulting entanglement bonds in the thermodynamic limit in Fig. 6(c). It can be clearly seen that the strongly and weakly entangled bonds alternate along the chain, as is expected for a dimerized phase.

Since the spin and charge modes are coupled and both

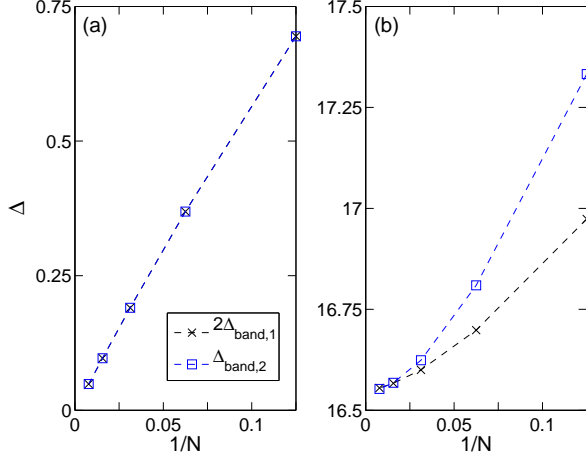


FIG. 5. (Color online) Finite-size scaling of the single-particle (Δ_{band}) and pair (Δ_{pair}) gap for the half-filled SU(2) Hubbard model at (a) $U = 0$ and (b) $U = 10$.

ξ	group number	ΔN_c	ΔS^z	Representative operator combination: $\langle \mathcal{T}_i^{(m)} \mathcal{T}_j^{(n)} \rangle$
2.32(4)	g1	0	$\{\pm 3, \pm 2, \pm 1\}$	$(c_1^\dagger c_2 n_3 n_4)_i (c_1 c_2^\dagger n_3 n_4)_j$
	g1	0	0	$(n_1 n_2 n_3 (1 - n_4))_i \times (n_1 n_2 (1 - n_3) n_4)_j$
1.92(3)	g2	0	$\{\pm 4, \pm 2, 0\}$	$(c_1^\dagger c_2^\dagger c_3 c_4)_i (c_1 c_2 c_3^\dagger c_4^\dagger)_j$
	g2	0	0	$(n_1 n_2 n_3 n_4)_i (n_1 n_2 n_3 n_4)_j$
1.25(4)	g3	± 1	$-\frac{3}{2}, \dots, \frac{3}{2}$	$(c_1^\dagger n_2 n_3 n_4)_i (c_1 n_2 n_3 n_4)_j$
0.88(6)	g4	± 1	$-\frac{1}{2}, \dots, \frac{1}{2}$	$(c_1^\dagger c_2^\dagger c_3 n_4)_i (c_1 c_2 c_3^\dagger n_4)_j$
0.61(8)	g5	± 2	$-2, \dots, 2$	$(c_1^\dagger c_2^\dagger n_3 n_4)_i (c_1 c_2 n_3 n_4)_j$
0.46(5)	g6	± 2	$\{\pm 3, \pm 1\}$	$(c_1^\dagger c_2^\dagger c_3^\dagger c_4)_i (c_1 c_2 c_3 c_4^\dagger)_j$
0.36(7)	g7	± 3	$-\frac{3}{2}, \dots, \frac{3}{2}$	$(c_1^\dagger c_2^\dagger c_3^\dagger n_4)_i (c_1 c_2 c_3 n_4)_j$
0.22(7)	g8	± 4	0	$(c_1^\dagger c_2^\dagger c_3^\dagger c_4^\dagger)_i (c_1 c_2 c_3 c_4)_j$
1.16(4)	I			Mutual Information

TABLE XII. Categorization of the generalized correlation functions for the half-filled SU(4) Hubbard model at $U = 10$.

modes are gapped, all generalized correlation functions decay exponentially, $G_{i,i+l} = \langle A_i B_{i+l} \rangle \sim \exp(-l/\xi)$ with ξ the decay length, as can be seen in Fig. 7. We group the generalized correlation functions into groups with the same decay length and find that they fall into eight groups, tabulated in Table XII. Since the generalized correlation functions describe all allowed transitions from an initial to a final state on a subsystem consisting of two sites, they encompass processes which correspond to spin and density correlations, as well as one- and multi-particle hopping on those two sites. The operators A_i in the correlation functions can now be characterized by eight independent parameters or by their proper symmetric and antisymmetric combinations. In analogy to results of conformal field theory, we expect that the decay lengths might be some simple function of the eight parameters. The possible values of ΔN_c and ΔS^z corresponding to the eight different groups are given

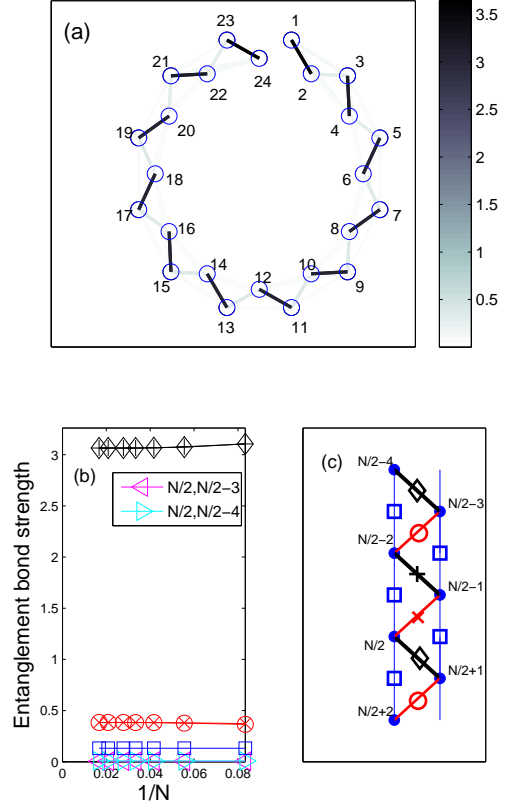


FIG. 6. (Color online) (a) Graphical representation of the components of the two-site mutual information for the SU(4) Hubbard model at half filling for $N = 24$ lattice sites. (b) Finite-size scaling of the leading entanglement bonds. (c) Entanglement pattern in the thermodynamic limit, with the width of the lines indicating the strength of the entanglement bonds. Entanglement bonds $I_{N/2, N/2-1}$, $I_{N/2, N/2+1}$, $I_{N/2-1, N/2-2}$, $I_{N/2+1, N/2+2}$, are denoted by the symbols \times , \diamond , \square , \circ , and $+$, respectively.

in Table XII. In general, the single-site transition operators, $\mathcal{T}_i^{(m)}$, can contain r fermion operators and $4 - r$ density-like operators with $r = 0, \dots, 4$. In addition, the r fermion operators are constructed from various combinations of creation and annihilation operators with different spin values. Some representative operator combinations are listed in the last column of Table XII. It is clear that the largest decay length corresponds to those generalized correlation functions where A_i does not change the particle number, i.e., $\Delta N_c = 0$. These are the slowest decaying correlation functions and are collected in groups 1 and 2. Group 2 also includes single-site transition operators with $r = 0$ fermion operators, and they are related to components of spin- and density-like conventional correlation functions. In the subsequent groups, as the single-site transition operator adds more and more particles to the system, the corresponding decay length decreases. The fastest decaying correlation functions correspond to $\Delta N_c = 4$, which is the maximum value. In addition to

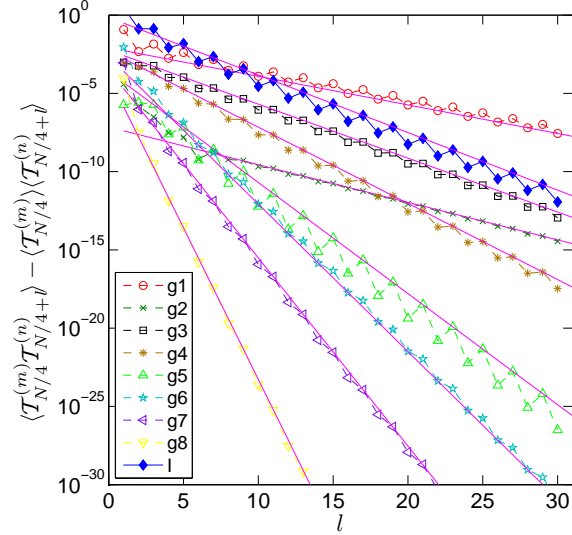


FIG. 7. (Color online) Similar to Fig. 4 but for the half-filled SU(4) Hubbard model with $N = 60$ sites for $U = 10$.

the strong ΔN_c dependence, the decay length also depends on ΔS^z because the related single-site transition operators describe different spin-flip processes. Single-site transition operators in group 3, 5, 7, and 8 contain $r = 1, 2, 3$, and 4 fermionic creation operators and $4 - r$ density-like operators, respectively. Their corresponding decay length drops systematically by a factor of two within our numerical error. A similar tendency is observed for groups 2, 4, and 6. It is worth reiterating that the decay length of $\langle \mathcal{T}_i^m \mathcal{T}_j^n \rangle$ depends only on the number of creation and annihilation operators, i.e., it is independent of the various combinations of the density-like operators by which the action of the fermion operators are weighted.

In order to further elucidate the origin of the behavior of the decay lengths of the different groups, we have calculated the band gaps formed by adding particles with different flavors as well as by adding particles with the same flavor. In both cases, the scaled gaps become equal in the thermodynamic limit, indicating that the level structure in the energy spectrum is uniformly spaced. A similar structure has been found in the spin sector as well. This behavior is shown for the half-filled SU(4) Hubbard model in Fig. 8. The fact that higher excitation gaps are integer multiples of the one-particle gap holds already for the finite chain with $N = 60$ lattice sites for which the decay lengths of the generalized correlation functions have been determined. These decay lengths are sometimes but not always integer multiples of each other. In addition, the observed trend for groups 3, 5, 7, and 8 and for groups 2, 4, and 6 is not linear. This can be understood by the fact that when band gaps are determined, the particles are added to the overall system. Thus, they are delocalized along the whole chain, whereas, for single-site transition operators with increas-

ing ΔN_c , more and more particles are added to a single-site subsystem. Higher excitations are possible in the latter case, so the decay length can decrease faster than the band gaps for the same ΔN_c values.

In summary, the slowest decaying generalized correlation functions belong to group 1, which have a decay length of $\xi_{g1} = 2.32$. The two-site mutual information also decays exponentially with a decay length $\xi_I = 1.16 = \xi_{g1}/2$. Therefore, it has half of the longest decay length of the slowest decaying generalized correlation function.

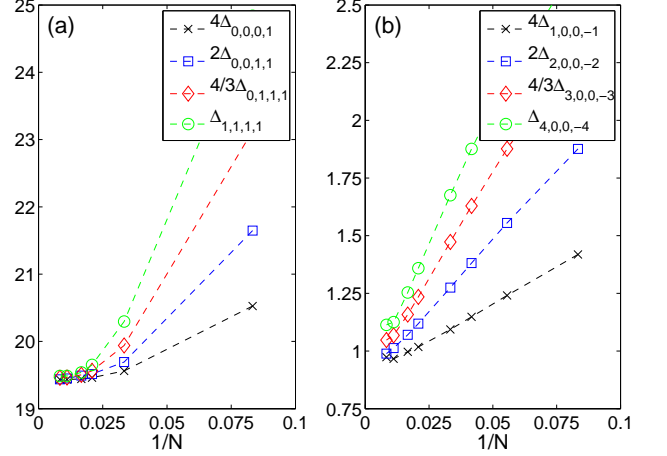


FIG. 8. (Color online) Finite-size scaling of (a) the band gaps related to adding one, two, three, or four particles to the system and (b) the spin gap for the half-filled SU(4) Hubbard model at $U = 10$. The gaps are denoted by $\Delta_{\Delta N_1, \Delta N_2, \Delta N_3, \Delta N_4}$, where the labels ΔN_σ show the change in the number of particles with spin σ .

A similar analysis for $f = 1/3$, i.e., the one-third-filled case, is presented in Fig. 9. Note that highly entangled three-site units are connected by a single entanglement bond. The strengths of the extrapolated values of the entanglement bonds show that next-nearest-neighbor entanglement is also important within the three-site entangled units. In addition, the entanglement map has left-right symmetry with respect to the mid-point of the three-site unit. The characterization of the correlation functions is summarized in Table XIII, and finite-size scaling of the relevant energy gaps is shown in Fig. 10. The scaled gaps become equal again in the thermodynamic limit, indicating an equidistant level structure in the energy spectrum of both the charge and spin sectors. According to Fig. 11 the decay length of the slowest decaying correlation function is $\xi_{g1} = 6.18(5)$, for which $\Delta N_c = 0$ and $\Delta S^z = 0$. The decay length of the two-site mutual information is $\xi_I = 3.02(4) = \xi_{g1}/2$.

We consider the case of higher flavor number, $n = 5$, in order to study even more extended spatial entanglement patterns. For $f = 1/4$, i.e., the quarter-filled case, a quadrimerized phase occurs, as can be seen in

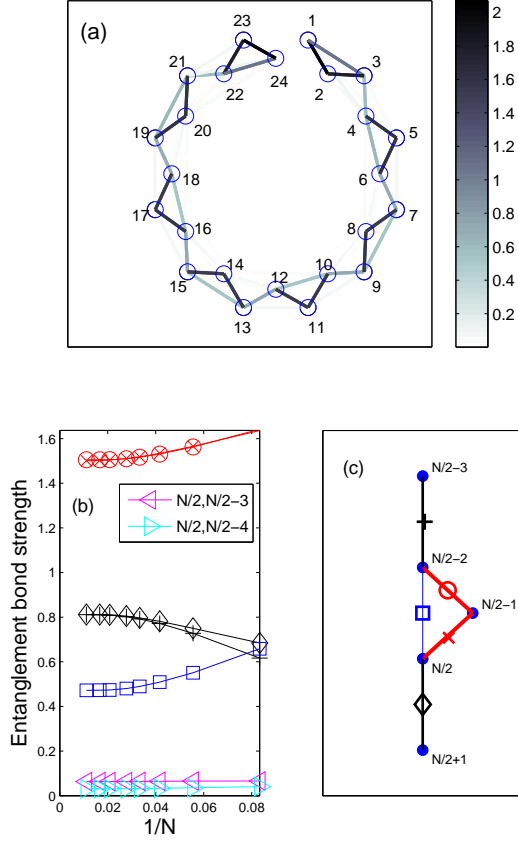


FIG. 9. (Color online) Similar to Fig. 6 but for the SU(4) Hubbard model at one-third-filling. The entanglement bonds $I_{N/2, N/2-1}$, $I_{N/2, N/2+1}$, $I_{N/2, N/2-2}$, $I_{N/2-1, N/2-2}$, $I_{N/2-2, N/2-3}$ are denoted by the symbols \times , \diamond , \square , \circ , and $+$, respectively.

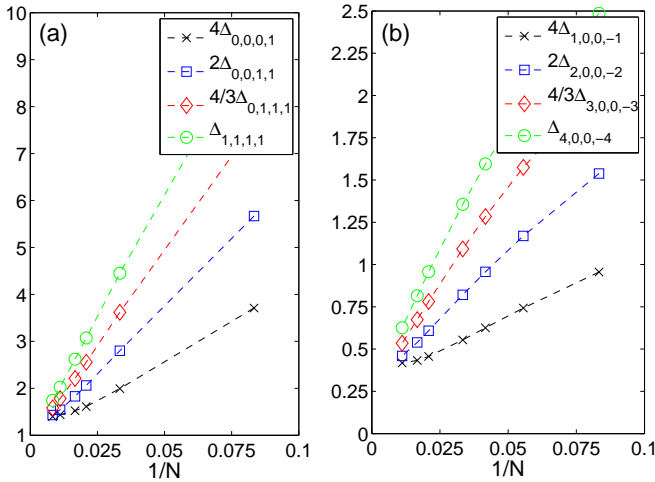


FIG. 10. (Color online) Similar to Fig. 8 but for the one-third-filled SU(4) Hubbard model at $U = 10$.

Fig. 12. The highly entangled four-site units are con-

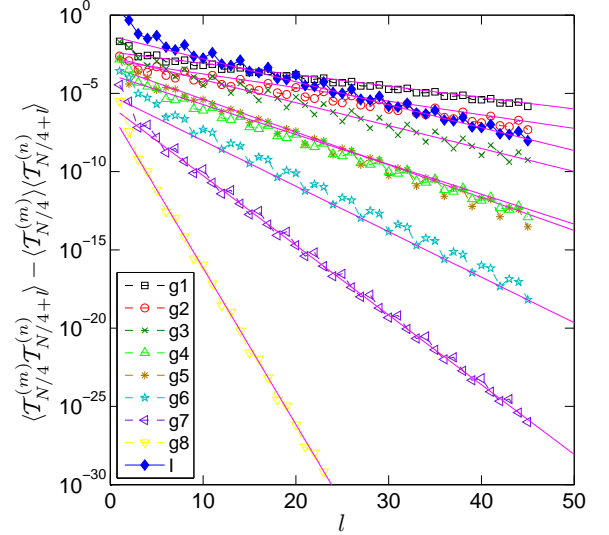


FIG. 11. (Color online) Similar to Fig. 4, but for the SU(4) Hubbard model at $f = 1/3$ filling and $U = 10$ calculated for a chain with $N = 90$ sites.

ξ	group number	ΔN_c	ΔS^z	Representative operator combination: $\langle \mathcal{T}_i^{(m)} \mathcal{T}_j^{(n)} \rangle$
6.18(5)	g1	± 1	$-\frac{3}{2}, \dots, \frac{3}{2}$	$(c_1^\dagger n_2 n_3 n_4)_i (c_1 n_2 n_3 n_4)_j$
4.54(4)	g2	0	$\{\pm 3, \pm 2, \pm 1\}$	$(c_1^\dagger c_2 n_3 n_4)_i (c_1 c_2^\dagger n_3 n_4)_j$
	g2	0	0	$(n_1 n_2 n_3 n_4)_i (n_1 n_2 n_3 n_4)_j$
3.03(3)	g3	± 1	$-\frac{7}{2}, \dots, \frac{7}{2}$	$(c_1^\dagger c_2^\dagger c_3 n_4)_i (c_1 c_2 c_3^\dagger n_4)_j$
2.27(3)	g4	± 2	$-2, \dots, 2$	$(c_1^\dagger c_2^\dagger n_3 n_4)_i (c_1 c_2 n_3 n_4)_j$
2.04(7)	g5	0	$\{\pm 4, \pm 2, 0\}$	$(c_1^\dagger c_2^\dagger c_3 c_4)_i (c_1 c_2 c_3^\dagger c_4^\dagger)_j$
1.49(3)	g6	± 2	$\{\pm 3, \pm 1\}$	$(c_1^\dagger c_2^\dagger c_3^\dagger c_4)_i (c_1 c_2 c_3 c_4^\dagger)_j$
1.0(2)	g7	± 3	$-\frac{3}{2}, \dots, \frac{3}{2}$	$(c_1^\dagger c_2^\dagger c_3^\dagger n_4)_i (c_1 c_2 c_3 n_4)_j$
0.45(4)	g8	± 4	0	$(c_1^\dagger c_2^\dagger c_3^\dagger c_4^\dagger)_i (c_1 c_2 c_3 c_4)_j$
3.02(4)	I			Mutual Information

TABLE XIII. Similar to Table XII but for the one-third-filled SU(4) Hubbard model at $U = 10$.

nected by single entanglement bonds. The strengths of the extrapolated values of the entanglement bonds indicate that next-nearest-neighbor entanglement is present within the four-site structure. In addition, second- and third-nearest-neighbor entanglement bonds also remain finite in the thermodynamic limit.

V. CONCLUSION

In this paper, we have formulated a method to characterize entanglement patterns in correlated systems. The measure that we use is the two-site mutual information, which is formed from the von Neumann entropy of the two-site and one-site density matrices. We have shown that the reduced density matrix of two- and three-site subsystems can be expressed in terms of two- and three-site generalized correlation functions related to all two- and three-site correlation functions based on site-local

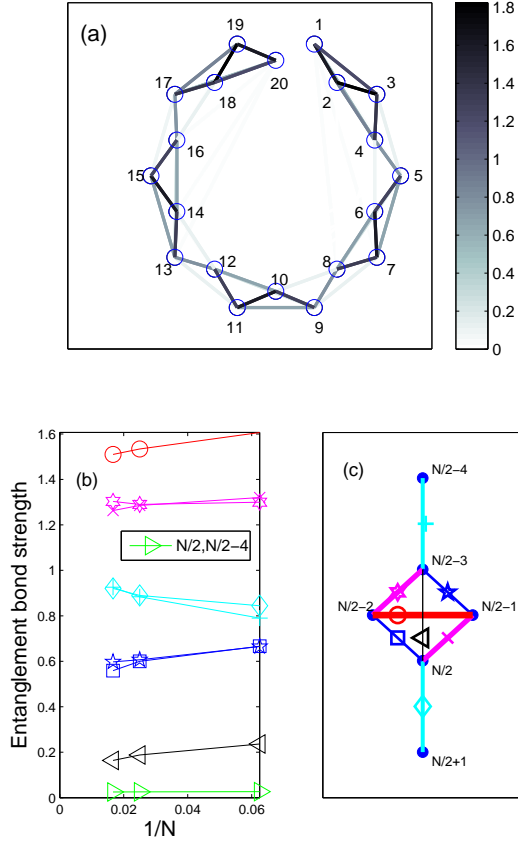


FIG. 12. (Color online) Similar to Fig. 6 but for the SU(5) Hubbard model at quarter-filling. Entanglement bonds $I_{N/2, N/2-1}$, $I_{N/2, N/2+1}$, $I_{N/2, N/2-2}$, $I_{N/2-1, N/2-2}$, $I_{N/2-1, N/2-3}$, $I_{N/2-2, N/2-3}$, $I_{N/2-3, N/2-4}$ are shown by symbols \times , \diamond , \square , \circ , \star , \blacktriangle , $+$, respectively.

operators. This procedure can be extended to n -site subsystem; thus the mutual information can be generalized to the n -site case. The major part of this work, in particular, the numerical calculations, concentrate on the two-site case.

For the $S = 1/2$ Heisenberg model, we have shown explicitly how the generalized correlation functions are constructed and have demonstrated that the dominant long-distance behavior of the mutual information follows the square of the most slowly decaying correlation function, which decays algebraically as the inverse of the distance. For the anisotropic Heisenberg model, both the generalized and the physical correlation functions can be divided into two groups that decay algebraically with different exponents. These exponents can be understood in terms of the known exact values for the transverse and longitudinal components of the spin correlations.

In Sec. IV, we have applied the methods to the one-dimensional SU(n)-symmetric generalized Hubbard model. For the half- and quarter-filled $n = 2$ case, we classify the generalized correlation functions into groups according to type of decay (algebraic or exponential)

and rapidity of decay (value of exponent and correlation length, respectively). The classification is consistent with the known excitation spectra at these points. We find that the two-site mutual information again decays as the square of the most slowly decaying correlation functions at long distances.

For higher spin models, i.e., $n = 3$ at half filling for large Coulomb interaction, we have confirmed the expected entanglement pattern of the dimerized ground state in which strong and weak bonds between nearest-neighbor pairs alternate on successive bonds. For $n = 4$ at one-third-filling, highly entangled three-site units are connected by a single entanglement bond. Within such three-site units, next-nearest-neighbor entanglement is also important. For an even higher number of flavors, $n = 5$, and at one-third-filling, we have again found three-site units with similar properties. On the other hand, at quarter filling, we have found highly entangled four-site units which are connected by single entanglement bonds. Within such entangled four-site units, second and third nearest-neighbor entanglement bonds also remain finite in the thermodynamic limit.

Therefore, based on our numerical results, we conclude that for $f = 1/q$ -filling and $q < n$, highly entangled q -site units are connected by single entanglement bonds in the ground state and within such entangled q -site units, first-, second-, and up to $q - 1$ -neighbor entanglement bonds also acquire finite strength in the thermodynamic limit. In addition, due to gaps in all excitation branches, all generalized correlation functions, together with the two-site mutual information, decay exponentially. Based on the decay length, they fall into several groups. We have found that their decay length depends on how the corresponding single-site transition operator changes the number of particles and the spin, consistent with the picture obtained from conformal field theory. The two-site mutual information again decays as the square of the most slowly decaying correlation functions; these correlation functions can also be used to identify the elementary excitation gap.

We remark that our method can easily be incorporated into a wide class of matrix-product-state- and tensor-network-state-based methods, of which the DMRG method is just one example. In particular, the method can be applied to higher-dimensional lattices to provide the basis for an optimization procedure to order matrix-product states and to construct efficient network topologies for tensor-network-state approaches.⁴⁷ Furthermore, our procedure can be utilized in other numerical methods in which one- and two-site operator expectation values are directly available. This is the case, for example, in the Configuration Interaction (CI) and Quantum Monte Carlo (QMC) techniques. Extension of the present work to study three-body entanglement is part of our planned future work.

ACKNOWLEDGMENTS

We thank Sz. Szalay, G. Ehlers, and F. Gebhard for useful discussions. This work was supported in part by Hungarian Research Fund (OTKA) through Grant

Nos. K100908 and NN110360. Ö.L. acknowledges support from the Alexander von Humboldt foundation and from ETH Zurich during his time as a visiting professor, and R.M.N. acknowledges support from the Deutsche Forschungsgemeinschaft (DFG) through grant no. NO 314/5-1 in Research Unit FOR 1807.

-
- ¹ S. Sachdev, *Quantum Phase Transitions*, 2nd ed., Cambridge Univ. Press, 2011.
- ² P. M. Chaikin and T. C. Lubensky, *Principles of Condensed Matter Physics*, Cambridge Univ. Press, 1995.
- ³ R. Horodecki, P. Horodecki, M. Horodecki, and K. Horodecki, *Rev. Mod. Phys.* **81**, 865 (2009).
- ⁴ Sz. Szalay, *Quantum entanglement in finite-dimensional Hilbert spaces (Ph.D. dissertation)*, arXiv:1302.4654 (2013).
- ⁵ L. Amico, R. Fazio, A. Osterloh, and V. Vedral, *Rev. Mod. Phys.* **80**, 517 (2008).
- ⁶ W. K. Wootters, *Phys. Rev. Lett.* **80**, 2245 (1998).
- ⁷ Vidal, Guifre, Entanglement monotones, *J. Mod. Opt.* **47**, 355 (2000).
- ⁸ M. Horodecki, *Quant. Inf. Comp.* **1**, 3, Rinton Press (2001)
- ⁹ M. Ohya and D. Petz, *Quantum Entropy and Its Use*, Springer Verlag (1993).
- ¹⁰ D. Petz, *Quantum Information Theory and Quantum Statistics*, Springer (2008).
- ¹¹ R. Horodecki, P. Horodecki, and M. Horodecki, *Phys. Lett. A* **210**, 377 (1996).
- ¹² A. Gabriel, V. Murg, B.C. Hiesmayr, arXiv:1309.1058 (2013).
- ¹³ G. Vidal, J. I. Latorre, E. Rico, and A. Kitaev, *Phys. Rev. Lett.* **90**, 227902 (2003).
- ¹⁴ P. Calabrese and J. Cardy, *J. Stat. Mech.: Theor. Exp.* P06002 (2004).
- ¹⁵ Ö. Legeza and J. Sólyom, *Phys. Rev. B* **68**, 195116 (2003).
- ¹⁶ G. Barcza, Ö. Legeza, K. H. Marti, M. Reiher, *Phys. Rev. A* **83**, 012508 (2011).
- ¹⁷ J. Vidal, G. Palacios, and R. Mosseri, *Phys. Rev. A* **69**, 022107 (2004); J. Vidal, R. Mosseri, and J. Dukelsky, *Phys. Rev. A* **69**, 054101 (2004).
- ¹⁸ M.-F. Yang, *Phys. Rev. A* **71**, 030302(R) (2005).
- ¹⁹ Ö. Legeza and J. Sólyom, *Phys. Rev. Lett.* **96**, 116401 (2006).
- ²⁰ N. Laflorencie, E. S. Sørensen, M.-S. Chang and I. Affleck, *Phys. Rev. Lett.* **96**, 100603 (2006).
- ²¹ Ö. Legeza, J. Sólyom, L. Tincani and R. M. Noack, *Phys. Rev. Lett.* **99**, 087203 (2007).
- ²² H. Braganca, E. Mascarenhas, G. I. Luiz, C. Duarte, R. G. Pereira, M. F. Santos, M. C. O. Aguiar, arXiv:1312.0619
- ²³ X. G. Wen, *Int. J. Mod. Phys. B* **4**, 239 (1990).
- ²⁴ A. Kitaev and J. Preskill, *Phys Rev Lett.* **96**, 110404 (2006).
- ²⁵ M. Levin and X.-G. Wen, *Phys Rev Lett.* **96**, 110405 (2006).
- ²⁶ J. Eisert, M. Cramer, M.B. Plenio, *Rev. Mod. Phys.* **82**, 277 (2010).
- ²⁷ A. Hamma and D. A. Lidar, *Phys. Rev. Lett.* **100**, 030502 (2008).
- ²⁸ F. Pollmann and A. M. Turner, *Phys. Rev. B* **86**, 125441 (2012).
- ²⁹ H.-C. Jiang, Z. Wang, L. Balents *Nature Physics* **8**, 902 (2012).
- ³⁰ Stefan Depenbrock, Ian P. McCulloch, and Ulrich Schollwöck, *Phys. Rev. Lett.* **109**, 067201 (2012).
- ³¹ S. Yan, D. A. Huse, and S. R. White, *Science* **332**, 1173-1176 (2011)
- ³² H. Li and F. D. M. Haldane. *Phys. Rev. Lett.* **101**, 010504 (2008).
- ³³ S. R. White, *Phys. Rev. Lett.* **69**, 2863 (1992); *Phys. Rev. B* **48**, 10345 (1993).
- ³⁴ U. Schollwöck, *Rev. Mod. Phys.* **77**, 259 (2005).
- ³⁵ R. M. Noack and S. R. Manmana, in *Diagonalization- and Numerical Renormalization-Group-Based Methods for Interacting Quantum Systems*, edited by A. Avella and F. Mancini (AIP, 2005), vol. 789, pp. 93-163.
- ³⁶ K. Hallberg, *Advances in Physics* **55**, pp 477-526 (2006).
- ³⁷ U. Schollwöck, *Ann. Phys. (NY)* **326**, 96 (2011).
- ³⁸ F. Verstraete and J. I. Cirac, arXiv:cond-mat/0407066v1 (2004).
- ³⁹ V. Murg, F. Verstraete, and J. I. Cirac, *Phys. Rev. A* **75**, 033605 (2007).
- ⁴⁰ V. Murg, F. Verstraete, and J. I. Cirac, *Phys. Rev. B* **79**, 195119 (2009).
- ⁴¹ F. Verstraete, J. I. Cirac and V. Murg, *Adv. Phys.* **57**, 143 (2008).
- ⁴² G. Vidal, *Phys. Rev. Lett.*, **101**, 110501 (2008).
- ⁴³ H. J. Changlani, J. M. Kinder, C. J. Umrigar, and G. K.-L. Chan, *Phys. Rev. B* **80**, 245116 (2009).
- ⁴⁴ K. H. Marti, B. Bauer, M. Reiher, M. Troyer, and F. Verstraete, *New J. Phys.* **12** 103008 (2010).
- ⁴⁵ V. Murg, F. Verstraete, Ö. Legeza, and R. M. Noack, *Phys. Rev. B* **82**, 205105 (2010).
- ⁴⁶ N. Nakatani and G. K.-L. Chan, *J. Chem. Phys.* **138**, 134113 (2013).
- ⁴⁷ V. Murg, F. Verstraete, R. Schneider, P. R. Nagy, Ö. Legeza, *J. Chem. Theory Comput.* **i11**, 1027 (2015). (2015).
- ⁴⁸ Ö. Legeza, J. Röder, and B. A. Hess, *Phys. Rev. B* **67**, 125114 (2003).
- ⁴⁹ W. Hackbusch, *Tensor Spaces and Numerical Tensor Calculus*, SSCM Vol. **42**, Springer, 2012.
- ⁵⁰ R. Dornier, V. Vedral, *Int. J. Mod. Phys. B* **27**, 1345017 (2013).
- ⁵¹ Ö. Legeza, F. Gebhard, and J. Rissler, *Phys. Rev. B* **74**, 195112 (2006).
- ⁵² J. Rissler, R. M. Noack, and S. R. White, *Chem. Phys.* **323**, 519 (2006).
- ⁵³ K. Boguslawski, K. H. Marti, Ö. Legeza, and M. Reiher, *J. Chem. Theory Comput.* **8**, 1970 (2012).
- ⁵⁴ K. Boguslawski, P. Tecmer, Ö. Legeza, and M. Reiher, *J. Phys. Chem. Lett.* **3**, 3129–3135 (2012).
- ⁵⁵ K. Boguslawski, P. Tecmer, G. Barcza, Ö. Legeza, and M. Reiher, *J. Chem. Theory Comp.* **9** 2959-2973 (2013).

- ⁵⁶ P. Tecmer, K. Boguslawski, Ö. Legeza, and M. Reiher, *Phys. Chem. Chem. Phys.* **16**, 719–727 (2014).
- ⁵⁷ M. M. Wolf, F. Verstraete, M. B. Hastings, and J. I. Cirac, *Phys. Rev. Lett.* **100**, 070502 (2008).
- ⁵⁸ S. Furukawa, V. Pasquier, and J. Shiraishi, *Phys. Rev. Lett.* **102**, 170602 (2009).
- ⁵⁹ N. Schuch, arXiv:13065551 (2013).
- ⁶⁰ M. L. Wall, *Quantum Many Body Physics of Ultracold Molecules in Optical Lattices* Springer, (2015). DOI 10.1007/978-3-319-14252-4.
- ⁶¹ Sz. Szalay and Z. Kökényesi, *Phys. Rev. A* **86**, 032341 (2012).
- ⁶² T. M. Cover and J. A. Thomas, *Elements of Information Theory*, John Wiley & Sons, New Jersey (1991).
- ⁶³ S. Montangero, M. Rizzi, V. Giovannetti, and R. Fazio, *Phys. Rev. B* **80**, 113103 (2009).
- ⁶⁴ K. Hallberg, X.Q.G. Wang, P. Horsch, A. Moreo, *Phys. Rev. Lett* **76**, 4955 (1996).
- ⁶⁵ K. Buchta, Ö. Legeza, E. Szirmai, and J. Sólyom, *Phys. Rev. B* **75**, 155108 (2007).
- ⁶⁶ E. Szirmai, Ö. Legeza, J. Sólyom, *Phys. Rev. B* **77**, 045106 (2008).
- ⁶⁷ R. Assaraf, P. Azaria, M. Caffarel, and P. Lecheminant, *Phys. Rev. B* **60**, 2299 (1999).
- ⁶⁸ S. R. Manmana, K. R. A. Hazzard, G. Chen, A. E. Feiguin, and A. M. Rey, *Phys. Rev. A* **85**, 053617 (2012).
- ⁶⁹ H. Frahm and V. E. Korepin, *Phys. Rev. B* **42**, 10 553 (1990).
- ⁷⁰ F. Woynarowich and H.-P. Ecker, *J. Phys. A:Math Gen.* **20**, 443 (1987).
- ⁷¹ N. M. Bogoliubov and V. E. Korepin, *Mod. Phys. Lett. B* **1**, 349 (1998); *Int. J. Mod. Phys. B* **3**, 427 (1989).
- ⁷² H. J. Schulz, *Int. J. Mod. Phys. B* **57** (1991).
- ⁷³ J. B. Marston and I. Affleck, *Phys. Rev. B* **39**, 11538 (1989).